Master Thesis

Modeling and Assessing an Energy-Aware Power-Supply for Wireless Sensor Nodes

Jesús Álvarez Álvarez

September 2009

Prof. Dr. Volker Turau

Institute of Telematics

Hamburg University of Technology

Declaration by Candidate

I, Jesús Álvarez Álvarez (student of Hamburg University of Technology, matriculation number 40071), hereby declare that this thesis is my own work and effort and that is has not been submitted anywhere for any award. Where other sources of information have been used, they have been acknowledged.

Hamburg, September 1st 2009.

Jesús Álvarez Álvarez

Abstract

Wireless sensors networks can be deployed in remote locations due to they do not need a fixed infrastructure. Therefore, energy scavenging systems are really important to provide the energy necessary to the sensor nodes and thus maximize its lifetime. This work presents the modeling and assessing of an energy-aware power-supply system for the Iris platform sensor. Theoretical models have been developed in order to estimate the energy in the energy storage supercapacitor depending on the incoming and outgoing energy. These models can be used to verify that the power-supply system provides enough energy to the sensor node under the most adverse weather conditions, and thus assuring the perpetual operation of the sensor nodes without human intervention. Also, these models will be implemented in a software module that makes possible the estimation of the sensor nodes' lifetime in function of their actual state of energy. The theoretical results given by these models have been compared with the results obtained with the real circuit. The comparison between both proves that the theoretical models are valid for the prediction of the future estate of energy based on the actual estate of energy.

Table of Contents

Chapter 1

Introduction

During the last decades, the computing devices have increases their capacities at the same time that they have become cheaper. Nowadays we can construct a mobile electronic device with the same benefits of personal computer from ten years ago. This has made possible the large deployment of small electronic devices in order to do tasks such as habitat monitoring, object tracking or traffic controlling [1-4]. When these devices share information wirelessly they form a wireless sensor network.

A wireless sensor node is an electronic device whose purpose is capturing data from the environment and using them in order to interact with the environment or sending them via wireless channels to a base station for further processing. Nowadays, these devices are powered by batteries that are able to provide the enough energy in order to work during several months [5]. A Wireless Sensor Networks if formed by tens to thousands of sensor nodes. These sensor nodes for a wireless network that use to share information and to perform distributed processing.

Since, the sensor networks can be deployed in remote locations, to reduce the power consumption is very important for prolong the lifetime of this type of devices [6]. Using techniques such as duty-cycling, which consist on turn on the radio only during shorts periods of time we can save energy and prolong the sensor node lifetime.

In the state of the art we can find several works that uses energy harvesting power-supply systems to prolong the lifetime of the sensor nodes. Those power circuits should be robust and operate without human intervention for many years [7]. Some of the current works that perform energy harvesting use rechargeable batteries in order to store the energy recollected. The maximum number of recharging cycles of the batteries limits the lifetime of the sensor nodes [8].

This work presents the modeling and assessing of an energy-aware power-supply system for the Iris platform sensor. The key design of this type of circuits is to prolong its lifetime in comparison with the use of the batteries, and when it is possible to obtain perpetual sensor node's lifetime.

We analyze the existing harvesting circuit and develop the theoretical models necessaries to estimate the future energy available for the sensor node. With the use of these models it is possible to simulate the behavior of the energy store in the supercapacitor based on the incoming and outgoing energy. Thus, we can assure under what conditions we can obtain perpetual lifetime.

These models will be implemented in a software module for the sensor node. The software developed will be able to predict the sensor node's lifetime in function of the current state of the energy stored in the supercapacitor.

Finally models and software developed will be evaluated in a real world scenario. The analysis and comparison of the real world versus the theoretical results will allow the validation of the models.

Chapter 2

State Of The Art

This chapter gives an introduction to wireless sensor networks (WSNs) and the main applications and challenges provided by this type of system. The characteristics of the sensor nodes that make up the WSN will be presented; in particular, the characteristics of the Iris sensor node will be explained. After giving an introduction to the WSN, the different solutions that have been proposed in order to obtain perpetual node's lifetime will be shown. Finally in the last section of the chapter the components that will integrate a generic power supply circuit will be shown.

2.1 Wireless Sensor Networks

Wireless sensor networks (WSN) consist of a large number of small, energy- and resource-constrained electronic devices that have sensors and actuators to monitor and modify the state of our physical world. These sensor nodes can communicate using a wireless channel. Besides, these devices have enough computational resources to perform distributed signal processing tasks [5]. The main application of the wireless sensor networks are: environmental monitoring, facility management, battle surveillance or traffic controlling [5-8].

Some of the characteristics of the sensor networks are shared with the ad-doc networks: they need for self-organization, time-variability in topology and wireless multi-hop operation. However, there are also important differences between sensor and ad-hoc networks that will be explained below.

The main task of a sensor node is to collaborate with other sensor nodes in sensing and controlling the physical environment. While sensor nodes remain in an assigned place, nodes in ad-hoc networks can move with their user [9].

Due to wireless sensor networks usually run only a single or very few applications, the application has knowledge about the data transported. Thus, this data can change or influence the behavior of applications and protocols. An example of this is the aggregation of data: instead of forwarding the individual packets, the forwarder can collect several packets and send only a packet that contains an aggregate value of those data. With this technique we obtain an important bandwidth and energy saving against a loss of information [10]

The number of nodes in ad-hoc networks is in the order of tens to hundreds, instead wireless sensor networks are foresee to have a higher amount of nodes [11].

In ad-hoc networks there are no distinguished nodes, and nodes communicate with arbitrary peer nodes. On the contrary in sensor networks there are few sink nodes present, to which the sensor nodes report their data. The communications happens either between neighboring sensor nodes or between sensor and sink nodes. Only a few times it happens that a sensor node which is more than a few hops away. The sink nodes can also configure and control the operation of the sensor nodes.

2.1.1 Challenges

Wireless sensor networks are currently receiving significant attention due to their indefinite potential. However, many research challenges exist in such systems. In this section, the main research challenges for wireless sensor networks will be outlined.

Most of these challenges are due to the wireless sensor networks has a high number of nodes communicating through a wireless channel in order to process a high amount of data that comes from different sources [12].

Real-World Protocols

Some of the solutions that are been developed in order to simulate the behavior of wireless sensor networks are not taken into account some important aspects about the wireless communication and the environment. Although this solutions work properly in simulation they cannot work so properly in practice. Thus it is necessary to develop novel protocols that take into account the realities that wireless sensor network behavior requires [13].

Real-Time

Wireless sensor networks can be used in environments the sensor data must be sent within time constraints. Nowadays very few results exist about real-time in wireless sensor networks. So, to expand the field application of the wireless sensor networks to environments that require real-time new results are needed in order to assure that WSNs work correctly with time constrains.

Programming abstractions

Increasing the level of abstraction for programmers of the wireless sensor networks, the expansion of the development and deployment of WSNs will be most significant. Nowadays the programmers of WSN are specialist in this field; raising the level of abstraction the general programmers could program new applications and protocols for the sensor nodes.

Analysis

Since wireless sensor networks are in the early development, few analytical results exist just now. The solutions are been built, tested and evaluated using simulators or testbeds. However, a scientific approach is required in order to analyze the designed systems before it is deployed. The analysis gives the results that assure that the system developed works correctly and efficiently [15]. Once analysis techniques are developed for the analysis of these systems, the must be validated in the real world.

Power Management

One of the main advantages of wireless sensor networks is the low-cost deployment. Instead, the sensor nodes sometimes are places in remote locations where the battery replacement is not a feasible solution [15]. Moreover, the application of many wireless sensor networks requires a long lifetime. Thus, it is a very important research topic to improve the energy efficiency of the wireless sensor networks as well as developing new systems that provides a form of energy surveillance. [16].

For those applications that require operating during longer durations without replacement of the batteries, several alternatives have been studied in order to provide

energy to the sensor nodes. These alternatives to powering the sensor nodes are based on converting the ambient energy from the environment into electrical energy to power the sensor nodes. Nowadays, the use of renewable energies is widely extended and developed in high power systems. However, the use of renewable energies to power the sensor nodes presents new challenges [17]. Usually the nature of the renewable energy is not continuous, so sensor nodes need to store the harvested energy. Also it is possible to use the sporadic available energy to quickly sense and transmit the data.

2.2 The Sensor Node

The basic elements of a wireless sensor network are the sensor nodes. Usually the sensor nodes have the following elements: the microcontroller, the transceiver, the external memory, the power source and one or more sensors [9]. The architecture equivalent of a sensor node is sketched in Figure 2.1.

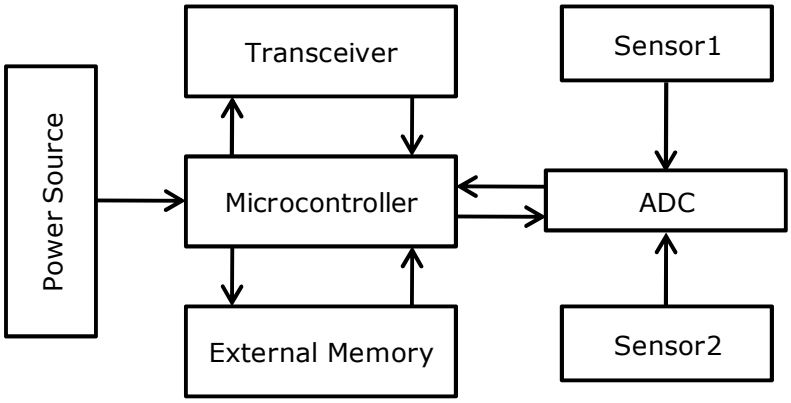

Figure 2.1: *Basic architecture of the sensor node*

2.2.1 Microcontroller

The microcontroller is the element that runs the application software and the protocol stack. Usually, the microcontrollers used in sensor nodes tend to be optimized for energy consumption and not for performance. Many of the sensor nodes are designed with 8-bit and 16-bit processors. Usually the clock rate, of the processor used, is a few tens of MHz [18, 19].

The Iris is the latest generation of sensor nodes from Crossbow Technology. The Iris node uses the Atmel RF230, IEEE 802.15.4 compliant, ZigBee-ready radio transceiver integrated with an Atmega1281 micro-controller. These enhancements provide up to three times improved radio range and twice the program memory over previous generation Mica sensor nodes [18, 20].

2.2.2 Wireless Transceiver

The function of the wireless transceiver is to perform the modulation, demodulation and transmission/reception of digital data over the wireless channel. When a sensor node is designed, the transceiver is chosen to optimize the energy consumption instead of priming the data throughput or packet error rates. This goal is achieved by low-power design and by choosing relatively small output powers. Moreover, reducing the data rates to the energy consumptions is lower [21].

Wireless transceivers operate in four different modes: transmit, receive, idle, and sleep. The first two modes: transmit and receive, consumes an amount of current in the range of milliamperes. In idle mode the power consumption is almost equal the same than in receive or transmit mode [22]. When the radio is not transmitting or receiving data, the best option is to shutdown the radio instead of change to the idle mode. Another important amount of energy is consumed during the switching from sleep mode to transmit mode.

2.2.3 External Memory

Both the type and the amount of memory for a sensor node depend on the application. Mainly, there are two types of memory: program memory, used for store the application in the sensor node, and user memory, used for storing the user and application data.

Based on an energy perspective, there are two types of memory: memory on chip and Flash memory. Access to the memory on chip is faster and consumes small amount of energy. This memory is used for store the program and also some of the user data. Flash memories are used due the storage capacity is higher than the on-chip memory. Also, the access to this type of memory consumes more power than the access to the on-chip

memory.

2.2.4 Sensors

The function of sensors is to produce a measure response to a physical change. The sensor circuitry transforms the physical condition in digital data using transducers and analog-to-digital converters. Examples for sensors are temperature, light, humidity [2-5]

2.2.5 Power Source

The power supply provides energy to the sensor node. Usually, the power source is a battery. In many WSN applications it is impractical or even impossible to replace or recharge the batteries of nodes due to the sensor nodes are placed in remote locations. Hence, the finite amount of energy implies a finite lifetime of the node. In the sensor node the processes that consume power are: sensing, communicating and data processing. More of the energy spending in the sensor node is for the data communication. Energy expenditure is less for sensing and data processing.

In the state of the art, some works have present sensor nodes are able to renew their energy from the environment using harvesting energy circuits, for example from solar [23], thermogenerator [24], vibrations [25] or temperature gradients [26]. Such systems, when combined with effective power-management techniques, can prolong the node lifetime significantly [27].

Table 2.1: *Power densities of energy harvesting technologies [28]*

Harvesting technology	**Power density**
Solar cells (outdoors at noon)	15 mW/cm^2
Piezoelectric (shoe inserts)	330 μW/cm^3
Vibration (small microwave oven)	116 μW/cm^3
Thermoelectric (10 _C gradient)	40 μW/cm^3
Acoustic noise (100 dB)	960 nW/cm^3

From Table 2.1, it is clear that solar energy is the most efficient renewable energy source available for sensor nodes deployed in outdoor locations. This makes it the best choice to power the sensor node, which consumes power on the order of several milliwatts. However, the design of an efficient energy harvesting power supply circuit involves important challenges. These challenges comes from the interaction of several factors, such as the characteristics of the energy sources, capacity of the energy storage elements used, power supply requirements, power management features [29]. Thus, it is essential to understand and exploit these factors in order to maximize the energy transfers from the harvesting modules efficiently.

2.3 Self-Sufficient Power Supply

One of the main limitations of wireless sensor networks are their energy storage resources and the power they obtain from their environment. Several solar powered designs have been developed to address this important problem. In this section, an introduction and analysis of the main works in this field will be provided.

In recent years, energy harvesting, especially solar energy harvesting has become increasingly important as a way to improve lifetime and decrease maintenance cost of WSNs. The solar energy harvesting for solar power systems is under active research [30]. Different institutions have developed several solar power designs with specific requirements such as lifetime, simplicity, flexibility (Table 2.2). For example, three leading design of solar power systems are: Prometheus [31], Heliomote [32] and Everlast [33]. These design show different points in the design space.

Table 2.2: *Examples of micro-solar power systems*

	Goal	**Key features**
Prometheus [31]	Lifetime, flexibility	Two-level storage, SW Charging
Heliomote [32]	Simplicity	HW Charging to NiMH batteries
Everlast [33]	Lifetime	MPP tracking

The architecture of **Prometheus** [31] has four main components: an energy source, buffer, charge controller, and consumer. This architecture uses as a primary buffer a supercapacitor, and a rechargeable battery as a second buffer. The primary operating mode of this system is to use a supercapacitor to collect environmental energy and to power the sensor node, while using the rechargeable battery as a reliable emergency backup.

The results obtained for the sensor node's lifetime show that to provide perpetual operation is possible for most wireless sensor networks applications where the duty cycle is 1% or less.

Heliomote [32] has a simple architecture that performs energy harvesting and storage. Besides this platform enables harvesting-aware operation by providing instantaneous solar and battery-state information.

The results obtained with Heliomote prove the viability of obtaining perpetual operation of outdoor sensor networks using solar energy harvesting.

Everlast [33] has a solar panel and a supercapacitor. It does not have a battery but does have a maximum power point tracking circuit. It charges a supercapacitor of 100 F while tracking the maximum power point of it solar panel. Its harvesting efficiency is much higher than Heliomote and Prometheus. However, to run the algorithm that allows the maximum power point tracking it requires an MCU.

2.3.1 System Architecture

In general, any solar-powered system consists of the following components: the external environment, the solar collector, energy storage and the sensor node (see Figure 2.2). The solar cell collects the solar energy from the environment and is stored in transferred to the energy storage by the solar collector circuit. The energy storage provides enough energy to the sensor node. The four components of a solar-powered sensor node interact with each other. The election of each component will determine the energy transfer between them as well as the behavior of the complete system.

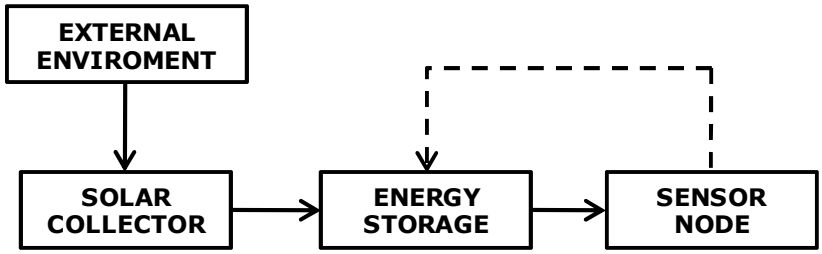

Figure 2.2: *Architecture of a micro-solar powered system*

Sensor Node

In a solar power system, the sensor node is the consumer of energy. The design and the election of the elements that form the power system are determined by the amount of energy consumed by the sensor node. As has been explained previously, the main causes of the power consumption are: radio communication, data processing and sensing. Since the sensor node consumes more energy when the wireless transceiver is awake than when it is sleep, a technique commonly known as duty-cycling is used to reduce the energy consumption of a sensor node. Duty cycle is the proportion of time during which a component or device is operated and can be expressed as a ratio or as a percentage [34].

Solar Collector

The solar collector includes two components: the solar cell and the energy harvesting circuit. The solar collector converts the solar radiation into electrical energy. The energy harvesting circuit fixes the output power of the solar cell and transfers this power to the energy storage element. This circuit performs the following three things: avoiding the back flow from energy storage to solar-cell, protecting the energy storage from overload, fixing the operating point for the solar cell. The amount of solar energy generated by the solar collector is determined by the following factors: solar radiation, solar-cell characteristics, and the operating point of solar-cell [35].

Energy Storage

Energy storage can consist of any number of storage elements grouped together in some configuration. The key challenge is to choose the combination of storage elements that maximize the efficiency of the energy transfer [43]. Besides maximizing the energy transfer, the next requirements must be taken into account:

- *Lifetime:* The lifetime of the energy storage is determined by the maximum charge or discharge cycles. The lifetime should be long enough to avoid frequent replacement.
- *Energy awareness:* The energy level is useful information that can improve the behavior of the WSNs in many ways, such as the routing protocol to choose the energy-efficient optimal route, the improvement of the load balance, and the reliability of data aggregation [37].
- *Prediction of stored energy:* The potential disruption of WSNs could happen because most of the nodes have insufficient energy to sustain the subsequent sensing and communication tasks. For this reason, the issue of estimating the energy level in the storage element is imperative [38].

2.4 Energy-Resource Estimation Techniques

Figure 2.1 shows the implementation of a generic architecture of a power supply circuit that allows intelligent energy transfers. In this section, the components and circuits that make up a power-supply system are presented. Also their behavior will be detailed using mathematical models.

2.4.1 Power Consumption by a Sensor Node

The sensor node influences the system's power consumption by changing its duty cycle. It can be modeled as a power sink of periodic pulses. The power consumption depends on three parameters: duty-cycle D, active mode current I_{active}, and sleep mode current I_{sleep}. The value of the duty-cycle D is chosen by the application, so it can adjust duty cycle intelligently. Assuming that the wakeup time is negligible, the average power

consumption is:

$$P_{AVG}(D) = V_{supply}\left(D \cdot I_{active} + (1-D) \cdot I_{sleep}\right) \quad 0 < D \leq 1 \tag{2.1}$$

In most sensor node's applications, the processor and radio run for a brief period of time, followed by a sleep cycle. During sleep, current consumption is in the range of microamperes as opposed to milliamperes during the active period. This results in low current draw during the most of the time, and short duration peaks of current in the range of milliamperes while the sensor node is processing, receiving and transmitting data.

2.4.2 Solar-cell

Solar energy is one of the most abundant and accessible types of renewable energy. We can find solar cell with different sizes that provides different voltage and currents. Usually, increasing the area or light intensity produces a proportionate increase in output current of the solar cell [35].

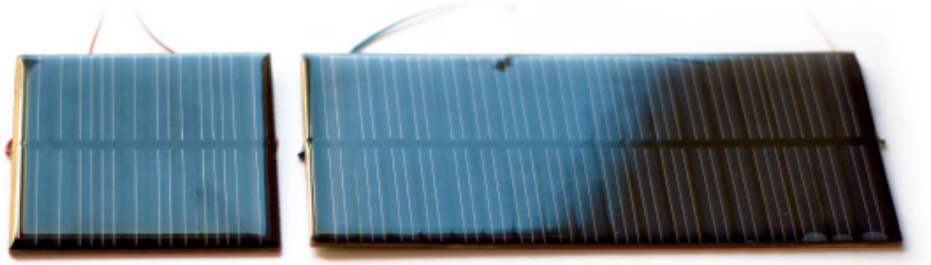

Figure 2.3: *Different types of solar cells with different size [39].*

We need that the solar cell will be able to provide enough energy to charge the energy storage element every day. The size of the solar cell should be determined based on how fast the energy storage element should be replenished; larger solar cells provide quicker charging. Thus, the size should be large enough to replenish the energy storage element even in the days with worst environmental conditions, such as during the winter with cloudy sky. The total power recollected by the solar cell depends on the latitude as well as the weather conditions, such as the cloudiness of the sky. In Table 2.3 it is shown the total radiation in different European cities [40].

Table 2.3: *Typical annual total of global radiation for different European cities [kWh/m^2]*

London	Hamburg	Berlin	Paris	Rome
945	980	1050	1130	1680

Equivalent circuit of a solar cell

In order to understand the electronic behavior of a solar cell, we will show the electronic equivalent circuit of a solar cell based on discrete components whose behavior is well known. An ideal solar cell may be modeled by a current source in parallel with a diode; in practice no solar cell is ideal, so a shunt resistance and a series resistance component are added to the model [41]. The resulting equivalent circuit of a solar cell is shown in Figure 2.4.

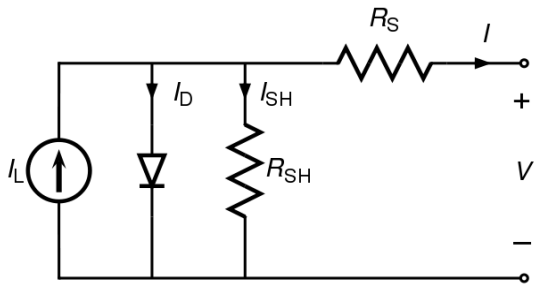

Figure 2.4: *Electrical equivalent circuit of a solar cell.*

Characteristic equation

From the equivalent circuit it is evident that the current produced by the solar cell is equal to that produced by the current source, minus that which flows through the diode, minus that which flows through the shunt resistor [41]. In the next equation it is shown the relationship between the solar cell parameters to the output current and voltage:

$$I = I_L - I_0\left(\exp\left[\frac{q(V + IR_S)}{nkT}\right] - 1\right) - \frac{V + IR_S}{R_{SH}} \qquad (2.2)$$

Where, I_0 is the reverse saturation current, n is the diode ideality factor (1 for an ideal diode) and $k \cdot T / q \approx 0.0259$ (volts) for silicon at 25°C.

For (2.2), given a particular operation voltage V the equation can be solved in order to obtain the output current I for that voltage V. However, since the equation involves I on both sides, has not general analytical solution, and it has to be solved using numerical methods. Figure 2.5 shows the solution of (2.2) for different operating voltage from zero Volts to V_{oc} (open circuit voltage).

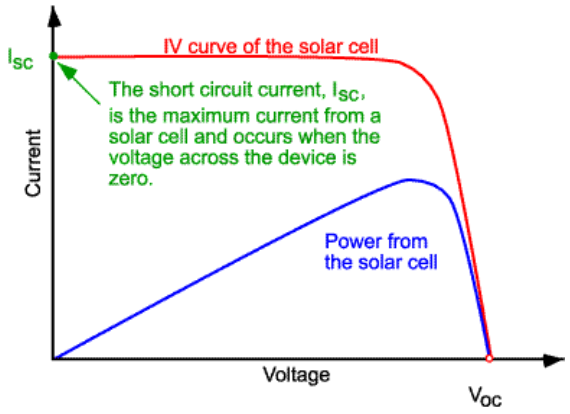

Figure 2.5: *Typical Characteristics of a solar cell*

Maximum Power Point (MPP)

The solar cell provides the maximum power when the product of I and V is the maximum. Since the solar irradiance may increase or decrease, the I-V curve changes in function of the solar radiation received. Thus, a solar cell can be described as a sequence of I-V curves with each I-V curve corresponding to a particular solar irradiance condition (Figure 2.6). The problem of finding the maximum power point is to locate the voltage operating point at which the solar cell provides the maximum output power when the light intensity changes.

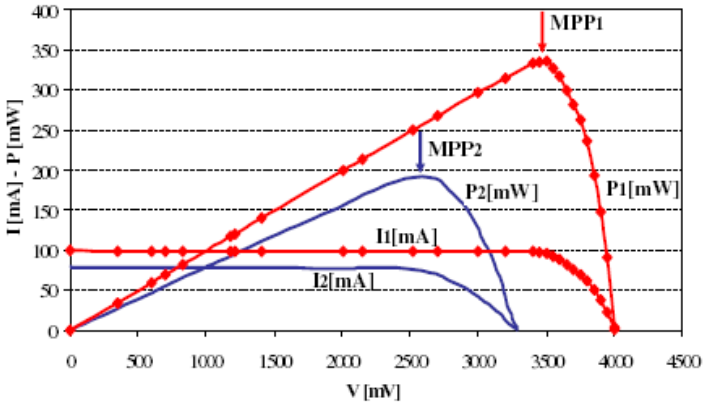

Figure 2.6: *Different curves I-V under different sunlight conditions [42].*

2.4.3 Supercapacitor

The source power that it is needed for a power supply system based on renewable energy needs to handle frequent charge cycles due to it buffers a variable incoming energy from the power source. Rechargeable batteries are typically rated for a few hundred charge cycles and, although they can endure many more charge cycles than the advertised rating, their lifetime is significantly decreased by frequent charge cycles. Supercapacitors have virtually infinite recharge cycles and are ideal for frequent pulsing applications. Historically supercapacitors are rarely used as energy storage element due to their limited capacity, but supercapacitors with large capacity are now a viable option. Nowadays it is possible to find supercapacitors with low cost, small size and high capacity. For example, we can find supercapacitors of 200F of several brands such as Panasonic or Samhwa with low prices [43, 44].

Figure 2.7: *Different supercapacitors compared with an AA battery [45].*

Supercapacitors are the only option that meets the goal of supply high levels of energy and handle frequent charge cycles without deteriorating over time itself. Supercapacitors vary from millifarads to hundreds of farads. To prolong the lifetime of the sensor node, the supercapacitor should be as large as possible.

The voltage in a supercapacitor is function of the capacity, the initial voltage and the current flows [46]:

$$V(t) = \frac{q(t)}{C} = \frac{1}{C}\int_{t0}^{t} I(\tau)d(\tau) + V(t_0) \qquad (2.3)$$

Taking the derivative of this, and multiplying by C, yields the derivative form that allows obtaining the flow current:

$$I(t) = \frac{dq(t)}{dt} = C\frac{dV(t)}{dt} \tag{2.4}$$

In order to obtain the energy balance in a system where a supercapacitor is present, we need to know the equation of the energy in the supercapacitor [46]. This equation is presented below:

$$E(t) = \frac{1}{2}CV^2(t) \tag{2.5}$$

Another important characteristic of the supercapacitor that is not presented in the previous equation is the leakage current. This is a flowing current that returns to ground through the supercapacitor. The leakage current depends on the supercapacitor voltage and the capacity. Usually, we cannot find the precise leakage of supercapacitors in the data sheet, so this function has to be determined experimentally. Figure 2.8 shows the leakage pattern of different supercapacitors. We observe that when the supercapacitors are fully charge, they suffer rapid discharge due to the leakage current.

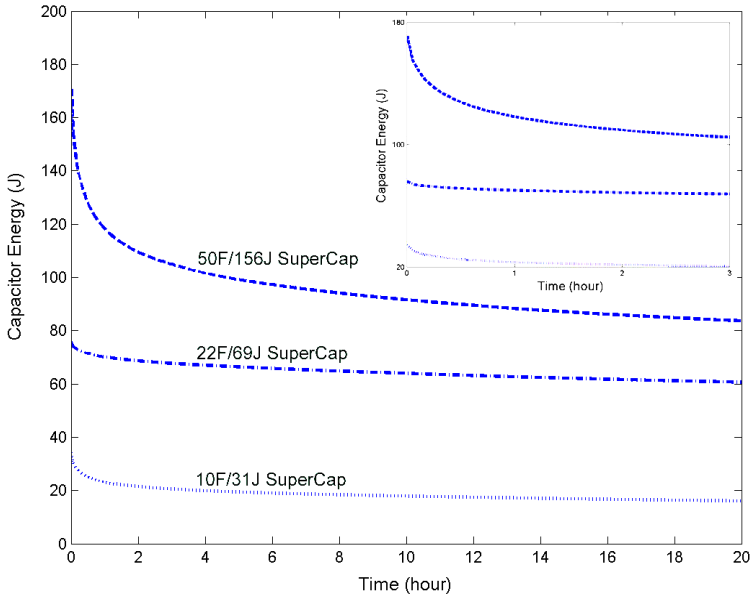

Figure 2.8: *Self-discharge of different supercapacitors [31].*

2.4.4 Voltage Converters

Many electronic circuits require a specific and constant voltage. Therefore, there is a need of converting a non stabilized voltage to a stabilized voltage with a certain level. If for example a source with non-constant tension, like a supercapacitor, for supplying a circuit with certain voltage requirements, a voltage conversion is necessary. One of the more efficient methods of voltage conversion is provided by the use of a switching converter. Usually, switching power supplies have an efficiency around 60-90% [47].

The main characteristics of a DC-DC converter are the range of the input voltage, the range of the output voltage, the maximum current that it can drop, and the efficiency [47]. If we have a circuit like the circuit of Figure 2.10, the efficiency is defined by the next equation:

$$\eta = \frac{P_{OUT}}{P_{\mathrm{IN}}} = \frac{V_{OUT} \cdot I_{IOUT}}{V_{\mathrm{IN}} \cdot I_{\mathrm{IN}}} \tag{2.6}$$

where V_{IN} is the input voltage, I_{IN} the input current and V_{OUT} is the output voltage and I_{OUT} is the output current.

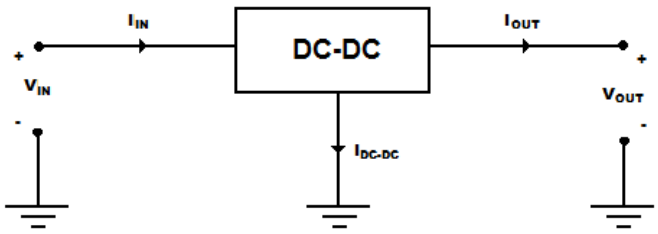

Figure 2.9: *Scheme of a DC-DC circuit.*

Chapter 3

Energy Estimation for Solar Harvesting Supply

Environmental energy is an attractive power source for powering wireless sensor networks. In the first part of this chapter, we present the design and elements of the power supply circuit for the Iris sensor node. In the second part, a detailed model for estimating the energy available for the sensor node will be developed. This model allows obtaining the energy stored in the supercapacitor in function of the incoming and the outgoing energy.

3.1 Analysis of the Existing Power Supply Circuit

The aim of this section is to study a self-sufficient energy supply for the Iris Sensor node design. The main requirement of this system is to provide enough power to the sensor node in order to obtain perpetual lifetime. Other requirements of this system are dimensions and weight of the entire system. These parameters will be minimized to ensure that the advantages of compactness and low weight of the Iris-node are maintained. It has been designed as a standard add-on board for the Iris Node design. The unused lines will be looped through, so the extension plug for additional components is available [45].

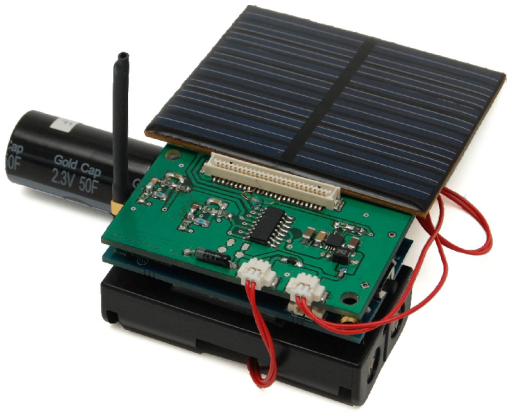

Figure 3.1: *Energy Harvesting Platform for the Iris node [48]*

The power supply circuit is based on the use of a solar cell in conjunction with a supercapacitor to harvest and store the solar energy. Besides another components are necessary to assure the proper energy transfer. These components are: Charging Unit, Discharge Unit and Status Unit. Figure 3.2 shows schematically the overall concept with these three components.

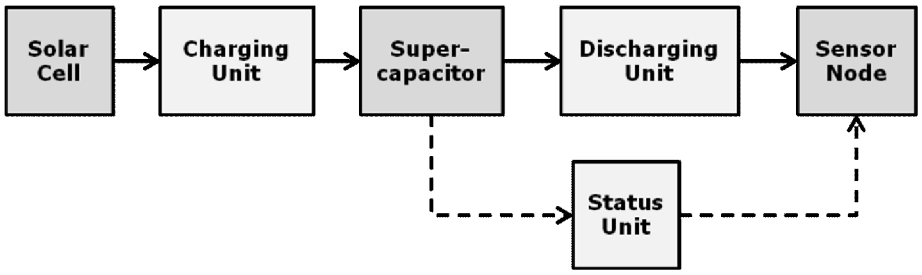

Figure 3.2: *Components of the power supply circuit.*

The Solar Cell

Thin-film photovoltaic cell is used as an energy harvesting subsystem. The size of the solar panel is 65 mm x 57 mm. At standard test conditions, the solar cells could generate 5 V open circuit voltage and 81 mA short-circuit current. The maximal output power is 405 mW at the optimal operating point [49].

The Charging Unit

The charging circuit is designed to ensure that the current generated by the solar cell is transferred to the supercapacitor. There is the possibility of charging the supercapacitor connecting the terminal of solar cell directly to the terminals of the supercapacitor.

Additionally, two points have to be taken into account. First, since the solar cell under no external light behaves like a diode, it could consume the energy stored in the supercapacitor. To avoid that, it is necessary to place a Diode between the solar cell and the supercapacitor. The best choice is to place a Schottky diode, since that diode has a low voltage between its terminals. Second, since the maximum output voltage of the solar cell is higher than the maximum voltage allowed in the supercapacitor, it is necessary to limit the maximum output voltage of the solar cell. This can be achieved through the use of a diode between the terminals of the solar cell. The best option is to use a Zener diode with a breakdown voltage as near as possible to the maximum supercapacitor voltage [45]. The circuit explained is shown in Figure 3.3.

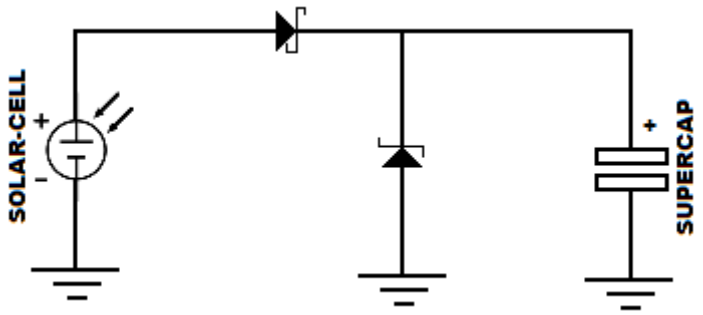

Figure 3.3: *Circuit for the connection of the solar cell with the supercapacitor*

The Supercapacitor

Energy storage is necessary due to the natural periodicity of sunlight. When the sunlight disappears, the energy storage subsystem powers the sensor node. The two choices of energy storage are rechargeable batteries and supercapacitors. Supercapacitors offer a higher lifetime in terms of charge-discharge cycles. We implement energy storage by using supercapacitors. The capacity of the supercapacitor is determined by the power consumption of the sensor node and duration of no sunlight period. The supercapacitors chosen for this system have been: GoldCaps from Panasonic [43] with a capacity of 22 F and 50 F with a maximum terminal voltage of 2.3 V; GreenCaps from Samhwa [44] with a capacity of 25 F, 50 F, 100 F and 200 F with a maximum terminal voltage of 2.7 V.

The Discharging Unit

The main purpose of the power supply circuit is to provide the sensor node the necessary energy to work correctly. According to the data given in [18] the Iris sensor node works with a voltage between 2.4 V and 3.3V. After the measurements in carried out in [50], it was shown that the minimum voltage for supplying the sensor node is 2.2 V. With the use of batteries the output voltage is relatively constant, but as the output voltage of the supercapacitor changes with the energy stored, it is necessary to use a voltage converter to provide a constant voltage.

The discharge unit consists of a DC-DC voltage converter [39]. The selection of the correct DC-DC converter is based on the next parameters: the range of the input voltage, the output voltage and the efficiency. The range of the input voltage should be as large as possible in order to assure that most of the energy stored in the supercapacitor can be used. The output voltage should be fixed at some voltage point between 2.4 V and 3.3V. Finally, the most important parameter in the election of the DC-DC converter is its efficiency. The first choice was a switching converter from Texas Instruments TPS61221 [47]. This device is capable to convert input voltages from 0.7 V to 5.5 V at a fixed output voltage of 3.3 V. The converter can be switched off by a featured enable pin. One of the main advantage of this circuit is that obtain a high efficiency for low output current. The efficiency versus the output current and input voltage, for an output voltage equal to 3.3 V, is shown in Figure 3.4. The rest of the important features of TPS61221 are indicated in Table 3.1.

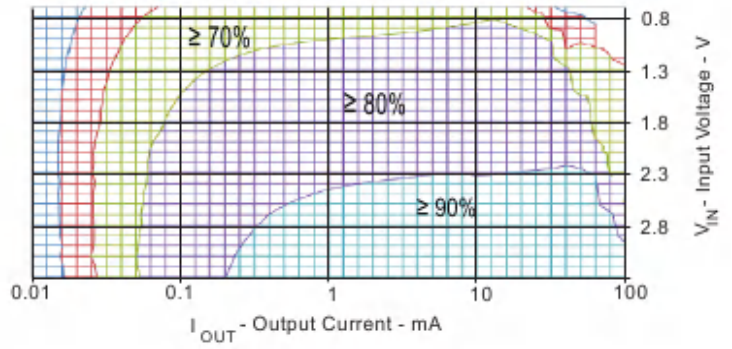

Figure 3.4: *Efficiency vs. Output Current and Input Voltage. (V_{OUT}=3.3 V)*

Table 3.1: *Characteristics of the selected DC-DC voltage converter [47]*

Manufacturer	**Texas Instruments**
Serial Number	TPS61221
I_{out} (Max)	50 mA
I_q (Typ)	5 mA
V_{in}(Min)	0.7 V
V_{in} (Max)	5.5 V
V_{out} (Max)	3.3 V
Switching frequency	2 MHz
Switch Current Limit	400 mA

The Status Unit

This part consists of a wire to connect the terminal of the supercapacitor to one of the ADC available in the sensor node. Knowing the voltage in the supercapacitor periodically, it is possible to know the current flow in the supercapacitor, the energy stored, and the sensor node's lifetime.

3.2 Energy Model for the Iris Sensor Node

The aim of this section is to present a detailed energy model for the power supply system. This model allows obtaining the energy stored in the supercapacitor in function of the incoming and the outgoing energy. Also, obtaining the sensor node's lifetime when we have no incoming energy is possible.

3.2.1 Power Generated by the Solar Cell

Using the model presented in Appendix 1, we can obtain the power generated by the solar cell under different external conditions. The power generated by a solar cell can be expressed as the following equation [35]:

$$P_{out} = max\{G_h \cdot \eta \cdot W \cdot L, \quad P_{MAX}\} \tag{3.1}$$

where G_h is the radiation received by a horizontal solar cell (see Appendix 1), η is the efficiency of the solar cell, W is the width of the solar cell, and L is the length of the

solar cell. Finally, as it was explained in section 2.4.2, P_{MAX} is the maximum output power that the solar cell can provide due to the effect of the internal diode.

From (3.23) we can obtain the output current of the solar cell knowing the operation voltage of it:

$$I_{out} = max\left\{\frac{G_h \cdot \eta \cdot W \cdot L}{V}, \quad I_{SC}\right\} \tag{3.2}$$

where V is the working voltage of the solar cell, and I_{SC} is maximum current that can be generated by the solar cell (short-circuit current).

3.2.2 Scavenging Efficiency

In order to transfer the energy generated by the solar cell to an energy storage element, such as a supercapacitor, several circuits can be used. The first option consists in connecting the solar cell directly to the supercapacitor. In order to avoid the energy transfer from the supercapacitor to the solar cell during the night it is necessary to place a diode between both. To minimize the energy consumed by this diode; it is recommendable to use a Schottky diode whose threshold voltage is low. Also it is necessary to place a diode between the terminals of the supercapacitor to avoid its overload. This circuit is show in Figure 3.3. With the use of this circuit the operation point of the solar cell is fixed by the supercapacitor voltage [39].

The second option in order to connect the solar cell with the supercapacitor is to use a DC-DC converter. Figure 3.5 shows the layout of a circuit that uses a DC-DC to connect the solar cell to the supercapacitor. With the use of this circuit it is possible to transfer energy from the solar cell to the supercapacitor even when the output voltage of the solar cell is lower than the voltage of the supercapacitor due to the use of the converter.

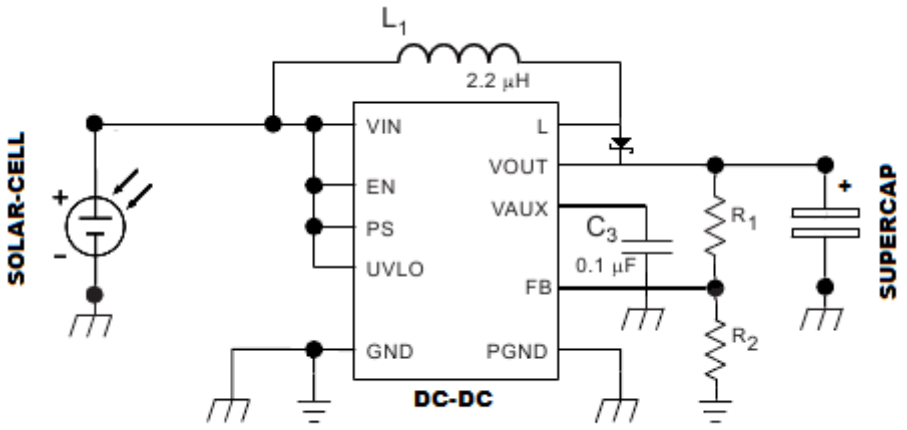

Figure 3.5: *Design for the connection between the solar cell and the supercapacitor.*

In order to obtain quantitative results of the energy transfer from the solar cell to the supercapacitor, a theoretical model has been developed for the previous circuits.

First of all, it is necessary to define the conversion efficiency as follows [51]:

$$\eta_{sc} = \frac{P_{transferred}}{P_{MPP}} \tag{3.3}$$

Where P_{MPP} is the power at the MPP and $P_{transferred}$ is the average power transferred to the energy buffer.

$$P_{MPP} = V_{MPP} \cdot I_{MPP} \tag{3.4}$$

Looking at (3.3) it is clear that only when the charging circuit works at the maximum power point we can achieve efficiencies close to 100% and losses are only caused by power dissipation of systems components.

3.3.3 Power Consumption by the Iris Sensor Node

The sensor node is the element in the circuit that may influence the power consumption by changing its duty-cycle. It can be modeled as a power sink of periodic pulses. The power consumption is dependent on three parameters: duty cycle D, active mode current I_{active}, and sleep mode current I_{sleep}. The average power consumption is given by (2.1).

For the Iris sensor node, according to [50] I_{active} is 18 mA and I_{sleep} is 18 µA. Also the voltage converter that we are using have a fixed output voltage of 3.3 V, so V_{supply} is equal to 3.3 V.

3.3.4 Energy Stored in the Supercapacitor

At this point, we are able to obtain the power generated by the solar cell using (3.1). Also it is possible to know the energy transferred from the solar cell to the supercapacitor by means of the scavenging efficiency. On the other hand, the power consumed by the sensor node can be obtained using (2.1). So, the final part of the energy model is to integrate all the parts in order to obtain the energy in the supercapacitor. Figure 3.6 shows the energy transfers between all the parts of a power supply system.

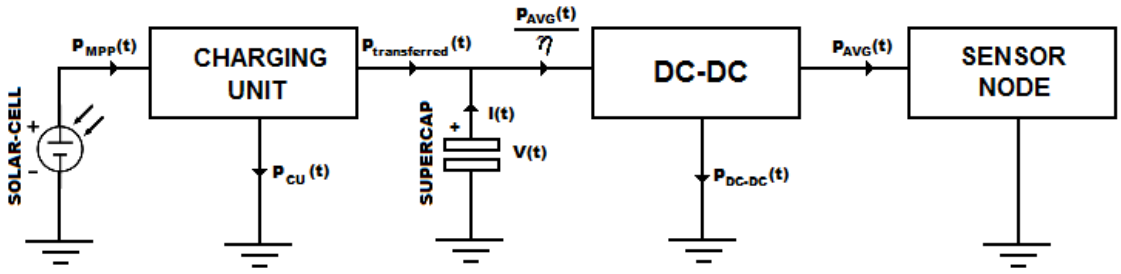

Figure 3.6: *Scheme of a power supply system for a sensor node.*

Looking at Figure 3.6, we can determine that the energy stored in the supercapacitor is equal to:

$$E(t) = \max\left\{ E_0 + \int_0^t P_{transferred}(\tau) - \frac{P_{AVG}(D)}{\eta} - P_{LEAK}(\tau) d\tau, \quad 0 \right\} \tag{3.5}$$

Where E_0 is the initial energy stored in the supercapacitor, $P_{transferred}(t)$ is the power transferred from the solar cell to the supercapacitor, $P_{AVG}(D)$ is the power consumed by the sensor node, η is the efficiency of the DC-DC converter and $P_{LEAK}(t)$ is the power lost in the supercapacitor due to the internal leakage current. Since $P_{AVG}(D)$ can be considered constant along the time, this equation can be expressed as follows:

$$E(t) = \max\left\{ E_0 + \int_0^t P_{transferred}(\tau)d\tau - \frac{P_{AVG}(D)}{\eta}t - \int_0^t P_{LEAK}(\tau)d\tau, \quad 0 \right\} \tag{3.6}$$

Equation (3.29) gives a model for the power supply system that allows obtaining the lifetime of a sensor node. The lifetime depends of the incoming energy from the solar cell, the energy the sensor node consumes, and the energy that is lost internally in the supercapacitor due to the leakage current. Assuming that the energy lost due the leakage current is neglected, and the incoming energy is null, it is possible to obtain a simple model for the sensor node's lifetime. From the following equation it is possible to obtain the sensor node's lifetime:

$$E(t) = \max\left\{ E_0 - \frac{P_{AVG}(D)}{\eta}t, \quad 0 \right\} \tag{3.7}$$

Using (2.5) we can change the values of energy in the supercapacitor by the terminal voltage, so Equation (3.7) becomes:

$$\frac{1}{2}CV^2(t) = \frac{1}{2}CV_0^2 - \frac{P_{AVG}(D)}{\eta}t \tag{3.8}$$

The sensor node's lifetime is determined by the minimum input working voltage of the DC-DC converter. Calling this voltage V_{min}, we obtain (3.32) that allows obtaining the lifetime in function of the initial voltage in the supercapacitor, the efficiency of the DC-DC converter, the minimum input working voltage of the DC-DC and the average power consumed by the sensor node.

$$T_{lifetime} = \frac{C \cdot \left(V_0^2 - V_{min}^2\right) \cdot \eta}{2 \cdot P_{AVG}(D)}; \quad 0 < D \le 1 \tag{3.9}$$

Since in a wireless sensor node to modify the duty-cycle dynamically is possible, we are interested in obtaining the maximum duty-cycle for a given lifetime. Using equations (3.27) and (3.32) it is possible to obtain the value of D for a given $T_{lifetime}$:

$$P_{AVG}(D) = \frac{C \cdot \left(V_0^2 - V_{min}^2\right) \cdot \eta}{2 \cdot T_{lifetime}}; \quad 0 < D \le 1 \tag{3.10}$$

Equation (2.1) can be rewritten as follows:

$$P_{AVG}(D) = V_{supply}\left(I_{sleep} + D \cdot \left(I_{active} - I_{sleep}\right)\right) \tag{3.11}$$

Substituting the value of $P_{AVG}(D)$ in (3.32) and solving the equation for D, we obtain:

$$D = \left(\frac{C \cdot \left(V_0^2 - V_{min}^2\right) \cdot \eta}{2 \cdot T_{lifetime} \cdot V_{supply}} - I_{sleep}\right) \frac{1}{I_{active} - I_{sleep}} \tag{3.12}$$

Due to usually the value of I_{active} is at least a hundred times greater than the value of I_{sleep}, the equation (3.35) can be simplified, obtaining the next equation:

$$D = \frac{C \cdot \left(V_0^2 - V_{min}^2\right) \cdot \eta}{2 \cdot T_{lifetime} \cdot V_{supply} \cdot I_{active}} - \frac{I_{sleep}}{I_{active}} \tag{3.13}$$

Chapter 4

Software Implementation

Wireless sensor networks are characterized by very tight code size and power constraints. In the first section of this chapter, we will present the TinyOS platform, and its characteristics. After that, we will develop a TinyOS module that allows obtaining the sensor node's lifetime based on the actual estate of energy of the supercapacitor.

4.1 TinyOS

TinyOS is an open source operating system designed for wireless sensor networks. TinyOS has a wide use by development communities, given their characteristics of being an open source project. It also supports different sensor node platforms, architectures foundation for application development.

The design of TinyOS is based on meeting the needs and characteristics of sensor networks, such as reduced memory size, low power consumption, diversity in design and uses. Also, TinyOS is optimized in terms of memory usage and energy efficiency.

TinyOS is built on a set of system components, which provide the foundation for building applications. Connecting these components, using a set of detailed specifications, is what ultimately will define an application. This model is essential in embedded systems to increase reliability without sacrificing performance.

TinyOS has migrated to multiple platforms, thus confirming its stability and performance verification. Furthermore applications have been developed capable of performing simulations, a wide community tool used to develop and test various algorithms and protocols.

Another feature of TinyOS is that the component model allows easy migration to other hardware. Moreover, migration is particularly important in sensor networks and new technologies are constantly emerging, where insurance system designers will want to explore the tradeoff between integration at the physical level, energy requirements, and system cost requirements key to optimization.

4.2 Software Design and Implementation

The power supply board offers a one-wire interface connected to one of the ADC of the microcontroller, so it is simple to obtain the value of the supercapacitor voltage and thus could obtain the energy or could estimate the sensor node's lifetime.

4.2.1 Objectives

The objectives of the module that we want develop is to have an independent interface that allows to obtain the actual state of energy of the power supply circuit, and through this value can calculate another output parameters such as the sensor node's lifetime based on the actual estate of energy of the supercapacitor. The software developed uses simple statements in order to utilize the power of the microcontroller to obtain the more precise results that is possible with a microcontroller without a float arithmetical unit.

One of the main purposes of this module is to report the status of the current energy and the lifetime to others services and protocols. Using this module other applications can change the routing path or increase the duty-cycle during certain hours of the day. Higher level software can take advantage of energy status knowledge. One example is to dynamically adjust duty cycle based on the energy in the supercapacitor. When there is energy enough, the sensor node can run at a higher duty cycle, and when the energy is low, it runs at a lower rate [52]. This is useful when the environmental energy is not equally distributed in the network. Nodes with higher exposure to environmental energy will increase their duty cycle to do more work (such as routing packets) while less exposed nodes will only perform minimal tasks.

4.2.2 Architecture

The component that we are developing is composed of two components: a module, called *SolarDriverC*, and a configuration, called *SolarDriverAppC*. In this case *SolarDriverAppC* is the configuration for the SolarDriver application. *SolarDriverAppC* is used to wire the *SolarDriverC* module to other components that the SolarDriver application requires.

As can be seen in Figure 4.4, this configuration provides an interface called *SolarDriver* and is composed of the *SolarDriverC* components along with *DemoSensor*, *SenseVoltage* and two timers. The remainder of the *SolarCellAppC* configuration consists of connecting interfaces used by components to interfaces provided by others. Carefully engineered TinyOS systems often have many layers of configurations, each of which refines the abstraction in simple way, building something robust with very little executable code. In Figure 4.1 it is displayed the diagram of the module developed and the modules that the SolarDriver use.

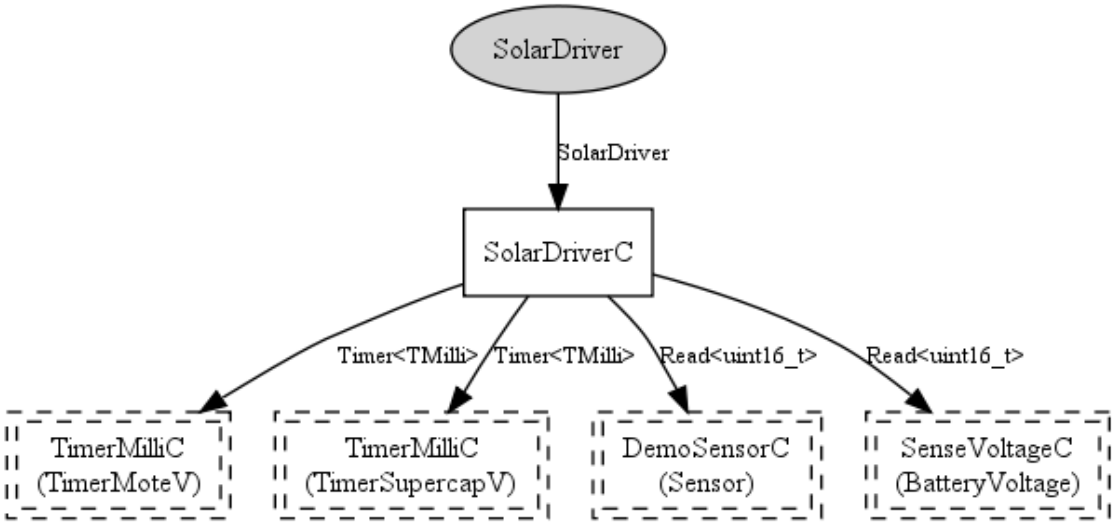

Figure 4.1: *Diagrams of the module developed for the Power Supply System*

The module that we developed has to read the supercapacitor voltage using one on the ADC available in the microcontroller. In this case, we are using the ADC1 to measure the voltage of the supercapacitor. In order to use this element, it is necessary to configure first the working mode of the ADC1. This has been done in the components *Atm1281Adc1C* and *Atm1281Adc1P*. Also, in this module it is possible to obtain the

battery voltage, so it has been used the module *SenseVoltageC* and *SenseVoltageP*. In order to follow the style rules given by tinyOS, all the access to the ADC have been carried out through the component *DemoSensorC*, so this component also have been modified in order to allow the reading of ADC1 and ADC0.

4.2.3 Design

Once the architecture of the program has been defined, the next step is the software design. This software will allow obtaining the desired output parameters in function of the supercapacitor voltage.

The first step is to know the model that allows obtaining the energy in the supercapacitor, the sensor node's lifetime and the maximum duty-cycle for a given runtime. We will use the simplified model explained in Section 3.3.4 to obtain these parameters. As it has been demonstrated in [48], the use a complex model, that takes into account the leakage current of the supercapacitors, only improve the exactitude of the predicted results when the voltage of the supercapacitor is near to the maximum voltage. Since the situation of the supercapacitor fully charged is not so usual, we can use the simple model.

The energy in the supercapacitor is given by (2.5). The equation that allows obtaining the sensor node's lifetime when the leakage current of the supercapacitor is neglected and when we have no incoming energy is given by (3.9). Finally, we use (3.13) to obtain the maximum duty-cycle for a given runtime.

From all the parameters needed in the energy model, we need to distinguish between the parameter that are going to be constant for all the applications, and those that can be change depending of the sensor node.

The constant parameters are: η, V_{IRIS}, I_{active}, I_{sleep} and V_{min}. These values can be defined in a header file as constants.

On the contrary the variables are: V, C, $T_{lifetime}$ and D. In this case the value of the supercapacitor voltage is given by the ADC, and re rest of the variables will be passed to the functions as parameters. At this point, we have defined the interface showed in Listing 4.1, in order to develop a module that implements this interface.

Listing 4.1: *Interface for querying the Iris Power Supply Circuit*

```
async command void measureMoteV();
async command void measureMoteVPeriodic(uint16_t period);
async command void measureSupercapV();
async command void measureSupercapVPeriodic(uint16_t period);
async command uint16_t estimateEnergy(uint16_t Capacity);
async command uint32_t estimateRuntime(uint16_t Capacity,
                                       uint16_t dutyCycle);
async command uint16_t estimateDutyCycle(uint16_t Capacity,
                                         uint16_t runtime);
async event void firedSupercapV(error_t result, uint16_t data);
async event void firedMoteV(error_t result, uint16_t data);
```

4.2.4 Implementation

The main problem to implement this module is that although most platforms support floating point numbers (float almost always, double sometimes), their arithmetic is in software rather than hardware, and due to that the energy consumption can be raised considerably. For this reason it is better to use integer arithmetic and integer variables.

Rather than the standard C names of *int*, *long*, or *char*, TinyOS code uses more explicit types, which declare their size. In reality, these map to the basic C types, but do so differently for different platforms. TinyOS code avoids using int, for example, because it is platform-specific. Additionally, TinyOS code often uses unsigned values heavily, as wrap-around to negative numbers can often lead to unintended consequences.

In order to obtain the highest precision as can be possible and also, taking into account to avoid the overflow, the data types for all the parameters and also the units have been chosen how can be seen in Table 4.1.

Table 4.1: *Data types and maximum values for the parameters of the module developed.*

Variable	**Type**	**Units**	**Max value**
Vbatt	uint16_t	mV	3300
Vsupercap	uint16_t	mV	2700
Capacity	*uint16_t*	*Farads*	*500*
DutyCycle	*uint16_t*	-	*1000*
time	*uint32_t*	*seconds*	*4.294967296e9*
Vmin	uint16_t	mV	1000
Isleep	uint16_t	µA	
Iawake	uint16_t	µA	50000000
eta	uint16_t	-	1000
estimatedEnergy	uint16_t	Joules	1000
estimatedRuntime	uint32_t	seconds	55976430
estimatedDutyCycle	uint16_t	-	1000

4.2.5 Software Test

Once the software have been developed, it is necessary to test that it works correctly. A new module called *TestSolarDriver* has been developed in order to test the module *SolarDriver*. This module uses the *SolarDriver* interface to obtain the energy, and the sensor node lifetime given by this interface in function of a theoretical value of the supercapacitor voltage.

Test carried out uses a variable theoretical supercapacitor voltage from 0.8 V to 2.7 V with a step of 0.05 V. Also it has been tested the output values for two different values of the duty-cycle: 1% and 100%. The rest of the values used for the test software are shown in Table 4.2.

Table 4.2: *Values of the constants during the software test [18].*

Constant	**Value**
η	0.7
V_{IRIS}	3.3 V
V_{min}	0.8 V
I_{SLEEP}	18 µA
I_{AWAKE}	18 mA
C	200 F
D	0.01, 0.1, 1

Figure 4.2 shows the values of the error between theoretical versus estimated by the module developed for the sensor node's lifetime. The results show that the module developed work correctly. The error due to the quantification of the input and output values is always lower than one second, so we can say that theoretical values and the predicted ones are practically the same.

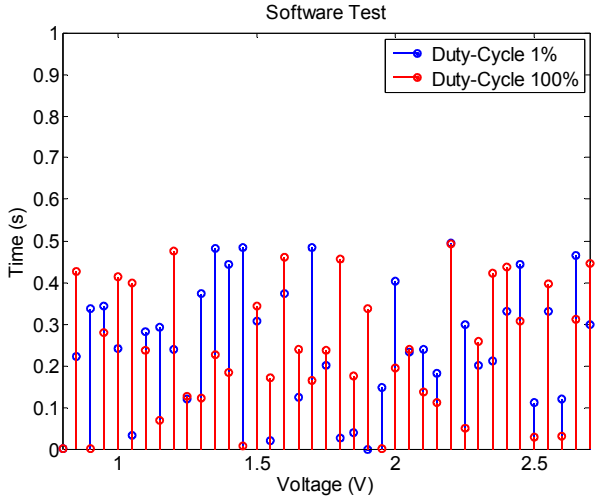

Figure 4.2: *Error between the theoretical values and the predicted ones by the software developed.*

Chapter 5

Evaluation

In this chapter, on the one hand, the theoretical concepts developed in the previous chapters will be evaluated. On the other hand, the hardware, together with the software developed, will be tested. Finally, the theoretical and the real results will be compared and discussed in the last sections of this chapter.

5.1 Theoretical Results

In this section the models developed in Chapter 3 will be used to simulate the power-supply system for the Iris sensor node.

In the real world test, a total number of eight supercapacitors have been used and tested. First of all, four supercapacitors of the brand Panasonic called GoldCaps, with capacities of 50 F and 22 F and a maximum voltage of 2.3 V. Second, four supercapacitors of the brand Samwha called GreenCaps, with capacities of 25 F, 50 F, 100 F, 200 F and a maximum voltage of 2.7 V. With the previous values we obtain the maximum energy stored in the supercapacitors using (2.5). Since the DC-DC converter only works when the input voltage is higher than 0.7 V, the energy stored in the supercapacitors that we can use is given by:

$$E_{usable} = \frac{1}{2} C\left(V_{\max}^2 - 0.7^2\right) \qquad (5.1)$$

Table 5.1 shows the maximum energy that can be stored in the different supercapacitors E_{max} used as well as the useable energy E_{usable}.

Table 5.1: *Characteristics of GoldCaps and GreenCaps*

	GoldCaps. V_{max} 2.3 V		***GreenCaps. V_{max} 2.7 V***			
Capacity (F)	**25**	**50**	**25**	**50**	**100**	**200**
E_{max} (J)	66.125	132.25	91.125	182.5	364.5	729
E_{usable} (J)	60	120	85	170	340	680

The solar cell used in this layout has a size of 65 mm x 57 mm, and an efficiency of 18%. At standard test conditions, the solar cells could generate 5 V open circuit voltage and 81 mA short-circuit current. The maximal output power is 405 mW at the optimal operating point.

5.1.1 Power Consumption by the Iris Sensor Node

The power is dependent on four parameters: voltage supply V_{supply}, duty-cycle D, active mode current I_{active}, and sleep mode current I_{sleep}. As it has been explained in Section 3.3.3, the average power consumption by the sensor node is given by (2.1).

For the Iris sensor node with the implemented power supply sensor board the values of the parameters are the next: $V_{supply} = 3.3V$, $I_{active} = 18mA$, $I_{sleep} = 18\mu A$ [18]. With these values, $P_{AVG}(D)$ for three different duty-cycles has been obtained. Since the average power consumption is constant in time, the energy consumed by the sensor node per day can be obtained as: $E_D = P_{AVG}(D)*3600*24$ *(Joules)*. The values of $P_{AVG}(D)$, and E_D are shown in Table 5.2 for three different duty-cycles.

Table 5.2: *Different Values of $P_{AVG}(D)$ and E_{DAY}*

D	**100%**	**10%**	**1%**
P_{AVG} (mW)	59.40	5.994	0.653
E_D (J)	5132	517.85	56.40

Taking into account the efficiency of the DC-DC converter is higher than $\eta=0.7$, the values of the power consumption of the discharging circuit are lower than $P_{AVG}(D)/\eta$. The values of $P_{AVG}(D)/\eta$, and E_{DAY} are shown in Table 5.2 for three different duty-cycles.

Table 5.3: *Different Values of $P_{AVG}(D)/\eta$ and E_{DAY}*

D	**100%**	**10%**	**1%**
P_{AVG}/η (mW)	84.86	8.563	0.933
E_{DAY} (J)	7332	739.8	80.57

5.1.2 Power Generated by the Solar Cell

In order to assure perpetual life of the Iris sensor node, the charging circuit and the supercapacitor chosen have to provide enough energy to the Iris sensor node, even under the worst weather conditions. These conditions are given for the day of the year with lowest hours of sun and with cloudy sky.

In Figure 5.1 the power generated by the solar cell has been obtained for January 1st and June 30th with different weather conditions, cloudy sky and clear sky. These results have been obtained using (3.1), with the next parameter of the solar cell: *efficiency 18%*, *width 57 mm*, *length 65 mm* and P_{max} *405 mW* [49]. For the day June 30th and clear sky, we can see the effect of the saturation of the output power of the solar cell. The theoretical values without saturation of the output power are plotted with dotted line.

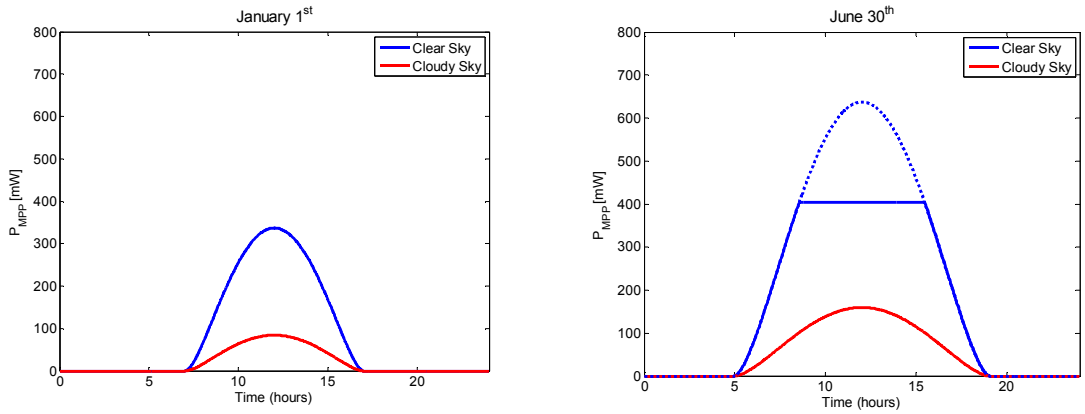

Figure 5.1: *Power generated by the solar cell at MPP for clear sky and cloudy sky.*

At this point it is possible to obtain the power generated by the solar cell for every day, and different weather conditions using (3.1). Integrating the value of $P_{MPP}(t)$ along the time we can obtain the energy generated by the solar cell in an interval of time.

$$E(t) = \int_{t_0}^{t_0+t} P_{MPP}(\tau)d\tau \tag{5.2}$$

The values of the energy harvested in a day have been obtained using (5.2) with *t = 24 hours*, for all the days of the year. These results are plotted in Figure 5.2. In this figure, it is also possible to see the effect limitation of the maximum output power for a solar cell. The dotted line shows the hypothetical energy generated in the case of not having saturation power.

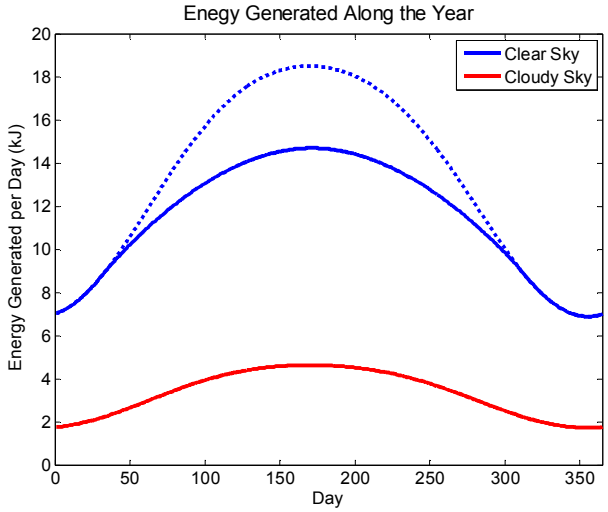

Figure 5.2: *Total energy generated in per day along the year.*

The results show that the minimum energy generated is approximately 1700 Joules for the days with less hours of sun and with cloudy sky. This value is more than twice of the maximum that can be stored in a GreenCap of 200 F, so it is possible to refill the supercapacitor energy every day. Also, this amount of energy is equal to the energy consumed by the sensor node for a duty-cycle of 25%.

5.1.3 Scavenging Efficiency

One of the main challenges of the solar power supply circuit is to manage efficiently the transfer energy from the solar cell to the supercapacitor. Conversion efficiency has been defined in (3.3).

When $P_{MPP}(t)$, the power generated by the solar cell at the maximum power point, is transferred to the supercapacitor, we can obtain the terminal voltage in the supercapacitor using its terminal voltage is given by:

$$V(t) = \min\left\{\sqrt{\frac{2 \cdot P_{MPP} \cdot t}{C}}; V_{\max}\right\} \tag{5.3}$$

When we connect the solar cell directly to the supercapacitor, the operation voltage of the solar cell is given by the terminal voltage of the supercapacitor. So using (2.4) we can express the power transferred as follows:

$$P_{transferred}(t) = V(t) \cdot I(t) = \left(\frac{1}{C}\int_0^t I(\tau)d\tau + V_0\right) \cdot I(t) \tag{5.4}$$

When we use a DC-DC converter to connect the solar cell with the supercapacitor, the power transferred evinces two different behaviors. When the input voltage is lower than the minimum working voltage of the DC-DC converter, the voltage converter is off and the supercapacitor are connected to solar cell through a diode, so the power transferred is given by (5.4). In contrast, when the input voltage is higher, the power transferred is equal to $P_{MPP}(t)$ multiplied by the efficiency of the DC-DC converter. This behavior is shown in (5.5).

$$V(t) = \min\left\{\sqrt{\frac{2 \cdot P_{MPP} \cdot \eta \cdot t}{C}}; V_{\max}\right\} \tag{5.5}$$

Figure 5.3 shows how efficient the described circuits are in replenishing a supercapacitor of 50 F. The green line shows the ideal trend: the supercapacitor is constantly refilled with the maximum available power P_{MPP}. The red line represents the charging behavior in case of a direct connection between the solar cell and the supercapacitor. The dashed blue line represents the charging behavior using a DC-DC converter with conversion efficiency equal to 0.75 and a minimum working voltage of 0.8 V.

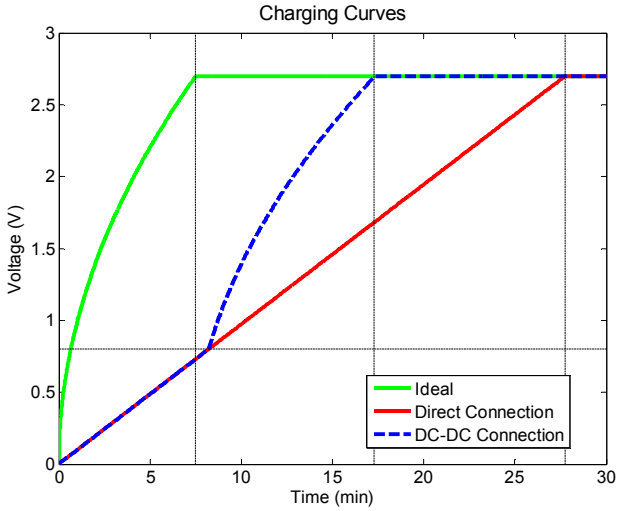

Figure 5.3: *Comparison between different charging curves.*

Figure 5.4 shows the same situation, but plots the efficiency, defined in (3.3), versus the voltage level of the supercapacitor. Looking at the blue line, it is even more evident that only when the energy level of the buffer is high enough to turn the DC/DC on, the scavenger can work properly and increase the efficiency.

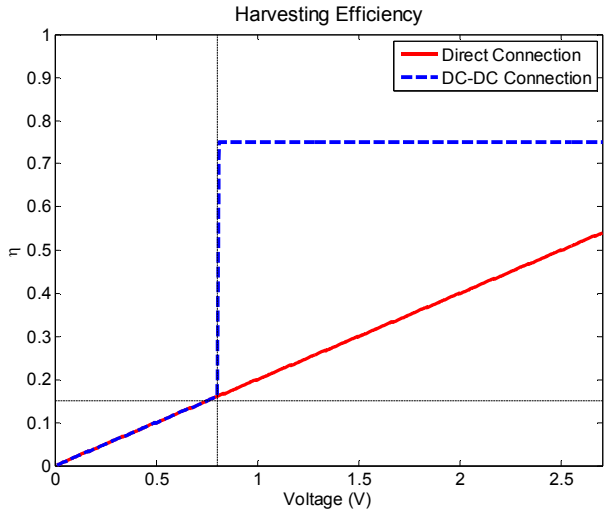

Figure 5.4: *Efficiency of different charging circuits.*

5.1.4 Simulation of the Complete System

In this section of the theoretical results, the simulations of the energy in the supercapacitor during several days will be shown. The results obtained show in which cases obtaining perpetual node lifetime is possible.

The results plotted in Figure 5.5 have been obtained using Equation (3.6) assuming that $P_{LEAK}(t)$ is neglected. To obtain the incoming energy from the solar cell Equation (3.1) has been used. In order to simplify the calculations the scavenging efficiency has been supposed constant and equal to 25%. This value has been obtained from Figure 5.4, taking the average efficiency. In order to obtain the output energy for the supercapacitor it has been used the data of the Iris sensor node, and we have assumed that the efficiency of the DC-DC converter is constant and equal to 0.7. Two different duty-cycles have been simulated, 10% and 1%.

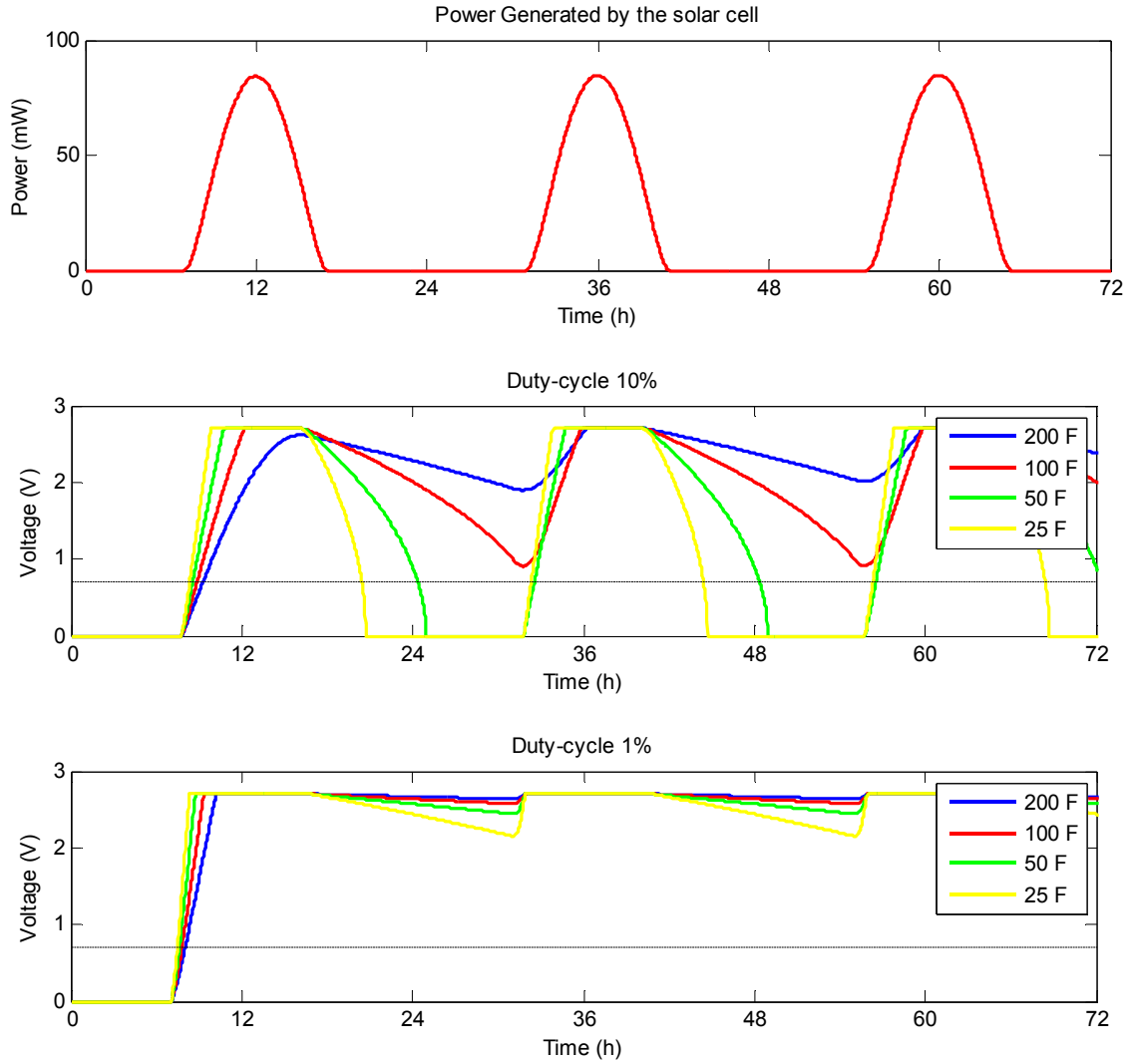

Figure 5.5: *Energy generated by the solar cell (top). Energy balance in the GreenCaps for a duty-cycle of 10% (centre) and 1% (bottom).*

Figure 5.5 (top) shows the incoming power from the solar cell for the first three days of the year and cloudy sky. Those are the worst environmental conditions for harvesting solar energy, so if the system works under those conditions, we can ensure that it will work for all the environmental conditions. In the center plot it is shown the voltage in the four GreenCaps with capacities of 200 F, 100 F, 50 F and 25 F for a duty-cycle of 10%. For the supercapacitor of 200 F and 100 F the voltage of the supercapacitor is always higher than 0.7 V, which ensures the perpetual lifetime of the sensor node if we use these supercapacitors. In the last plot, only the duty-cycle has been modified with respect to the previous plot. In this case perpetual sensor node lifetime is ensured for all the supercapacitors.

5.2 Hardware Evaluation

In this section the realistic results that have been obtained from the existing power supply board for the Iris sensor node are shown ad discussed. Due to this board is not finished yet, the test only shows the discharge behavior of the supercapacitor together with the evaluation of the software developed for estimating the sensor node lifetime.

5.2.1 Discharging Circuit Evaluation

The existing circuit seems to work correctly. A variable input voltage of at least 0.7 V produces the desired output voltage of 3.3 V. In order to test the circuit two experimental measurements have been carried out. First the input has been connected to an input variable voltage from 0 V to 2.7 V and the output voltage of the circuit has been measured. Secondly, the input has been connected to a variable voltage from 2.7 V to 0 V. The results of these experiments are shown in the figure 5.7.

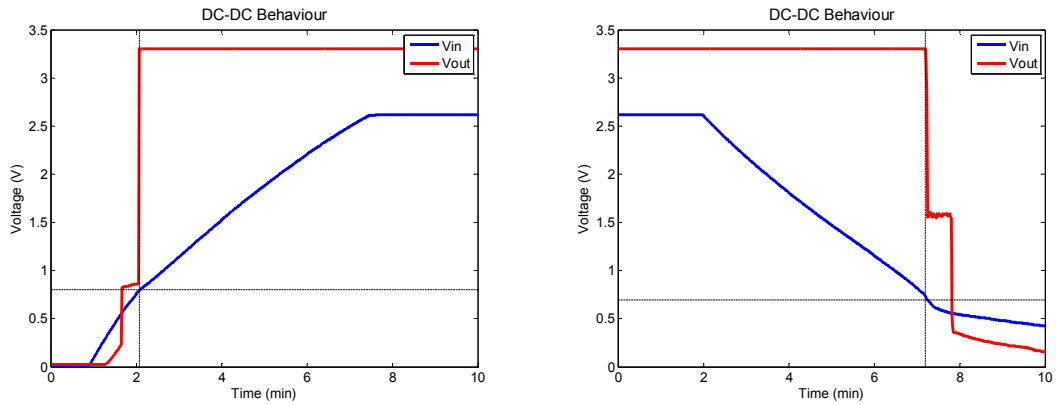

Figure 5.6: *Experimental arrangement for the functional verification of the DC-DC converter*

Figure 5.6 (left) shows that from about 0.8 V input voltage the converter provides the desired output voltage of 3.3 V. The analysis of the voltage gradient in falling voltage in Figure 5.6 (right) provides similar results with the difference that the voltage converter works down to 0.7 V.

An important factor of the DC-DC converter is its efficiency under different input voltage and output current. To obtain this parameter, the circuit has been tested for different duty cycles. The input of the circuit has been connected to a supercapacitor of 50 F and the output of the circuit has been the Iris sensor node. Since the current drawn by the sensor node is known, it is possible to obtain the current delivered by the supercapacitor and thus obtaining the efficiency of the circuit, as it is shown in (2.6).

For the power-supply circuit: V_{OUT} is 3.3V, I_{OUT} can be obtained in function of the duty-cycle, V_{IN} is the voltage of the supercapacitor and I_{IN} can be obtained using (2.4):

In Figure 5.7 the voltage of the supercapacitor of 50 it is shown, for duty-cycles of 100%, 10% and 1%. In addition, the current dropped from the supercapacitor is displayed.

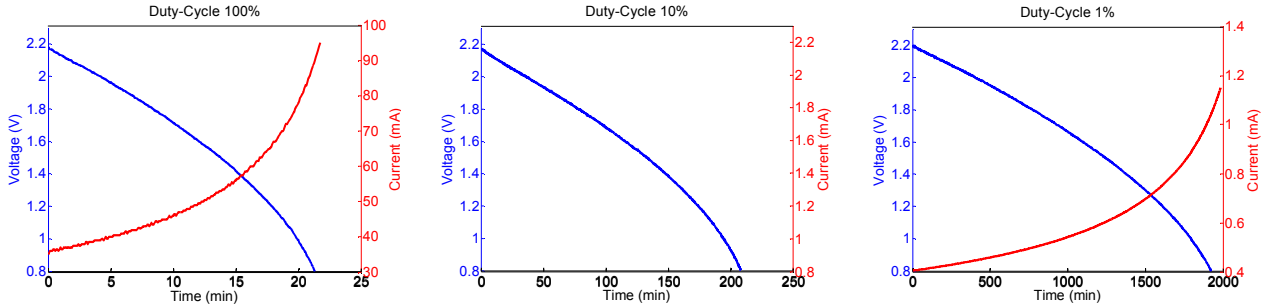

***Figure 5.7**: Voltage (red line) and current drawn from the 50 F GoldCap for different Duty-Cycles: 100% (left), 10% (centre) and 1% (right).*

Using Equation (2.6) the values of the average efficiency for the three duty-cycles have been obtained, and these values are almost constant and equal to $\eta=0.76$ for a duty-cycle of 100%, $\eta=0.75$ for a duty-cycle of 10% and $\eta=0.73$ for a duty-cycle of 1%.

Supercapacitors Self-Discharge

The leakage function $P_{LEAK}(t)$ of supercapacitors often needs to be determined experimentally. Figure 5.8 shows the leakage pattern of eight supercapacitors we tested under isolation. They all experience rapid leakage when fully charged, and slow leakage when the energy stored is lower than approximately 85% of the maximum energy. This means that when the supercapacitors are fully charged, the voltage will decrease rapidly until this value is reached. Afterwards, the terminal voltage will decrease very slowly.

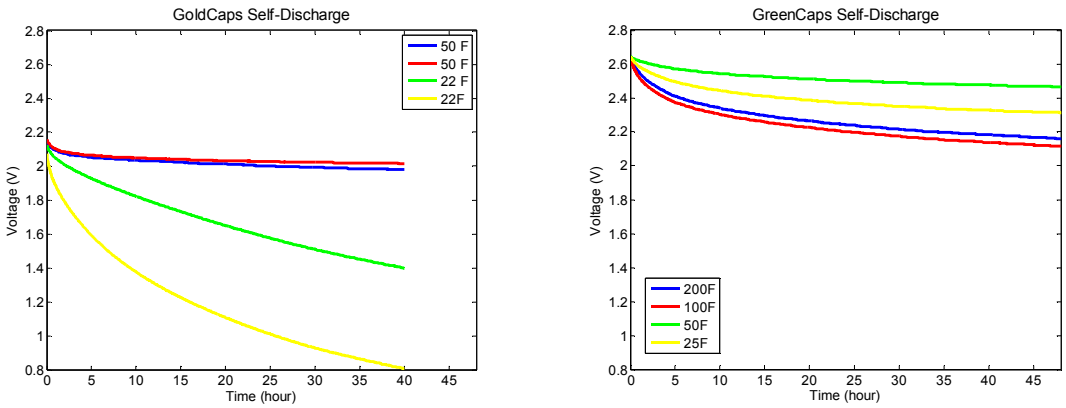

***Figure 5.8:** (Left) GoldCap self-discharge. (Right) GreenCap self-discharge*

Supercapacitor behavior

To prolong the lifetime of the sensor node, the supercapacitor should be as large as possible. In order to see the relation between the sensor node's lifetime, the capacity of the supercapacitors, and the efficiency of the voltage converter, all the supercapacitor have been tested using the Discharging Circuit displayed in Figure 5.9.

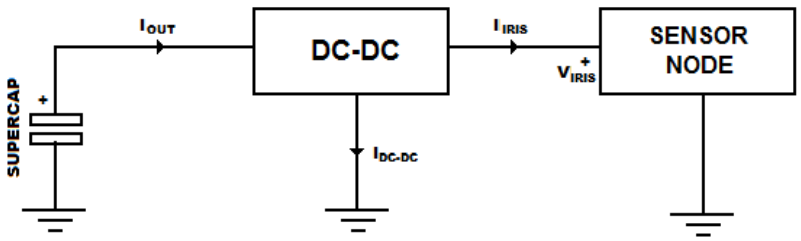

Figure 5.9: *Layout of the discharge circuit.*

Four GoldCaps and four GreenCaps have been tested. Two GoldCaps with capacity of 50 F and two with capacity of 22 F have been tested. GreenCaps have capacities of 200 F 100 F, 50 F and 25 F. Tests have been made for duty-cycles of 100%, 10% and 1%, and the results are shown in Figure 5.10. The results show the effect of the efficiency of the DC-DC converter. When the duty-cycle is lower, the efficiency of the DC-DC converter is worse, so the value of $T_{lifetime}/D$ decreases. Another important effect that can be observed in the graphics is the effect of the leakage current. This effect has particular importance when the duty-cycle is low and when the supercapacitor voltage is near to the maximum terminal voltage. On the contrary, when the supercapacitor voltage is lower than approximately 85% of the capacity, this effect can be neglected.

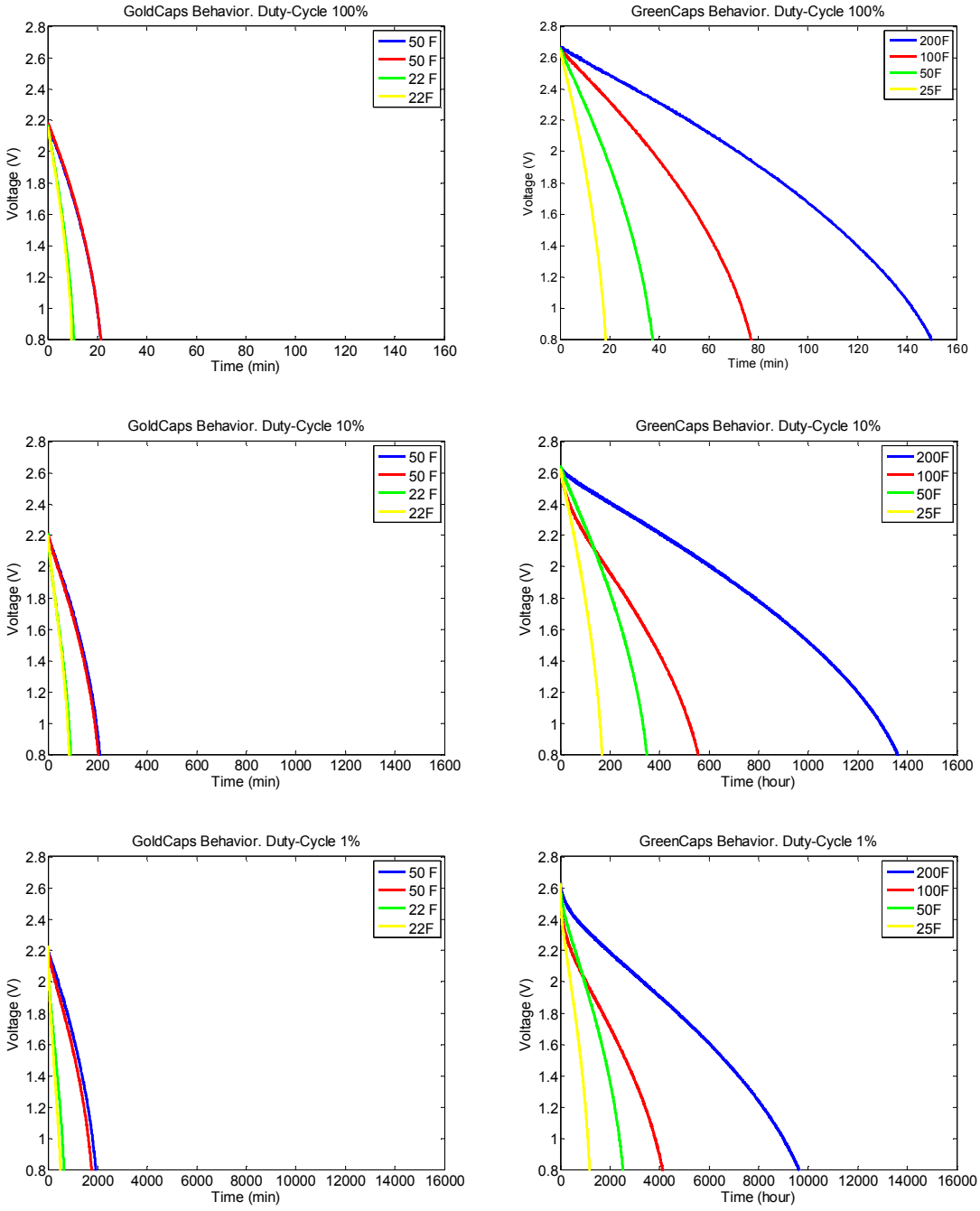

Figure 5.10: *GoldCap and GreenCap behavior*

5.2.2 Charging Circuit Test

In this section, since the existing power supply circuit does not have implemented the charging circuit yet, it will be evaluated a hypothetical charging circuit.

The circuits that have been tested are shown in Figure 5.11. First circuit is used as monitor circuit in order to obtain the output power in function of the solar radiation. It has only a solar cell connected to a resistance in order to measure the solar radiation received by the solar cell. Second circuit implements the connection of the solar cell to the supercapacitor. When the duty-cycle of the sensor is 1%, it draws a current of 0.2 mA. To simulate this behavior, the supercapacitor has been connected to a resistance of 10 kΩ. This resistance draws a current between 0.1 mA and 0.2 mA when the supercapacitor voltage is between 1 V and 2 V.

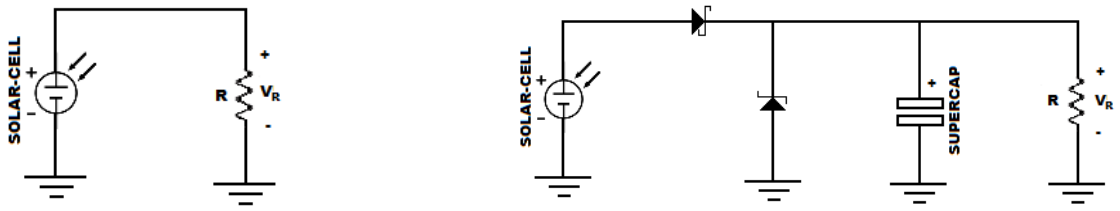

Figure 5.11: *Layout of the circuits used for testing the solar cell.*

With the use of two solar cells at the same time, one that works as light monitor and the other that is used to charge the supercapacitor, it is possible to make a comparison between the theoretical results, and the real results that are obtained. Due to weather conditions are a random variable it is impossible to predict with exactitude if the sky is going to be clear or cloudy. Due to that, in Figure 5.12 the real results obtained with the circuit of Figure 5.11 Left (blue line), and also the theoretical values for clear sky (green line) and cloudy sky (red line) are displayed.

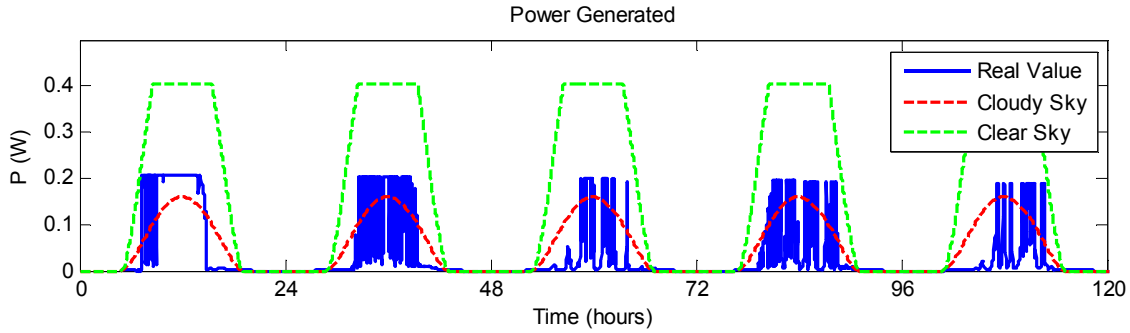

Figure 5.12: *Output power generated by the solar cell vs. theoretical values at MPP.*

The difference between the real results and the theoretical ones are due to the theoretical results are obtained for a solar cell working at maximum power transfer point, but in the real circuit the working point can be far away from the MPP. With the circuit that we are using the working point is fixed by the external resistance, and due to the output impedance of the solar cell varies with the solar radiation does not exists an adaptation between these two impedances, so the circuit does not transfer all the power generated by the solar cell to the external resistance.

With the values from the output current of the solar cell, we can obtain the energy harvested during a day using (5.2). In Figure 5.12 is plotted the accumulated energy along the day for the results from realistic hardware test (blue line), for theoretical values when the sky is cloudy (red line) and for theoretical values when the sky is clear (green line).

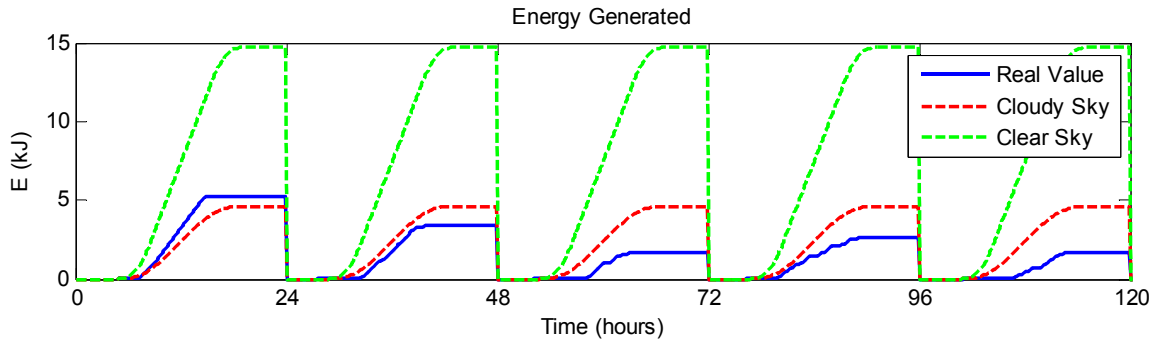

Figure 5.13: *Accumulated energy generated by the solar cell.*

Lastly, the two circuits of Figure 5.11 will be tested at the same time. The circuit on the right uses a GreenCap of 50F connected to the solar cell and a resistance of 10 kΩ (see Figure 5.11). The value of the reverse voltage of the Zener diode is 2.4 V in order to avoid the overload of the supercapacitor. In Figure 5.14 are displayed the values of the solar power harvested by the solar cell used as monitor, and in Figure 5.15 the voltage in the GreenCap of 50 F is displayed.

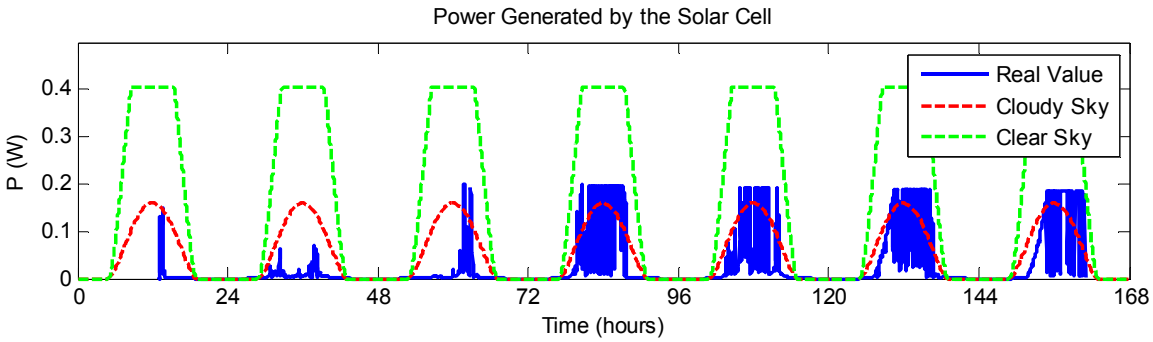

Figure 5.14: *Total energy generated by the solar cell vs. theoretical values.*

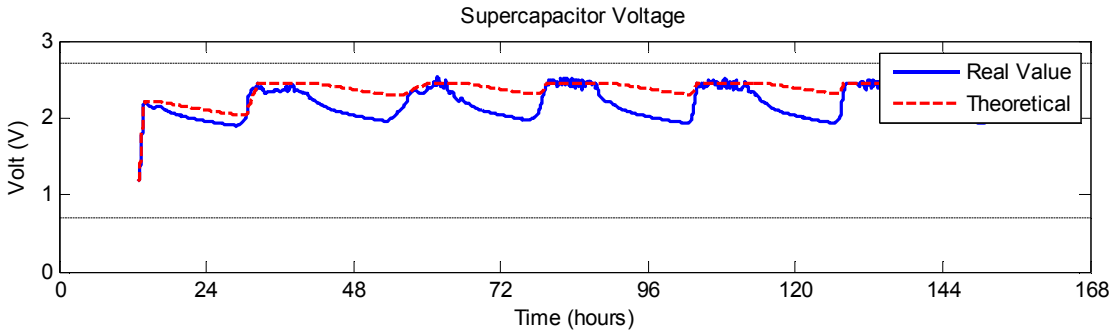

Figure 5.15: *Voltage in the GreenCap of 50 F.*

Comparing the two graphics, when the output power is higher in Figure 5.14, in Figure 5.15 we can observe how the supercapacitor replenishes faster. Also this plot shows that with the use of this charging unit, the supercapacitor replenish its energy every day, so perpetual lifetime of the sensor node can be ensured.

5.2.3 Status Unit Evaluation

In this section, the software developed in Chapter 4 for estimating the sensor node's lifetime is tested and evaluated. A total number of six tests have been carried out, three with a GreenCap of 200 F and three with a GreenCap of 25 F. For both GreenCaps the duty-cycle have been 100%, 10% and 1%. The efficiency has been 0.73 for 1% duty-cycle, 0.75 for 10% duty-cycle and 0.76 for 100% duty-cycle according to section 5.2.1.

In Figure 5.16 all the results obtained from the test are plotted. For a 100% duty-cycle, the error between the real values of the sensor node lifetime and the estimated values is small and almost constant along the time. For a 10% duty-cycle, we can observe the error firstly decreases and then increases. This is due to the efficiency of the DC-DC converter is not perfectly constant but changes a little with the input voltage. Lastly, for a duty-cycle of 1% the effect of the leakage current in the supercapacitors is observed clearly. At the begin of the test, when the supercapacitor voltage is near to the maximum voltage, the error between the real lifetime and the predicted values is high, but when the voltage is lower, this error is lower too, and almost constant.

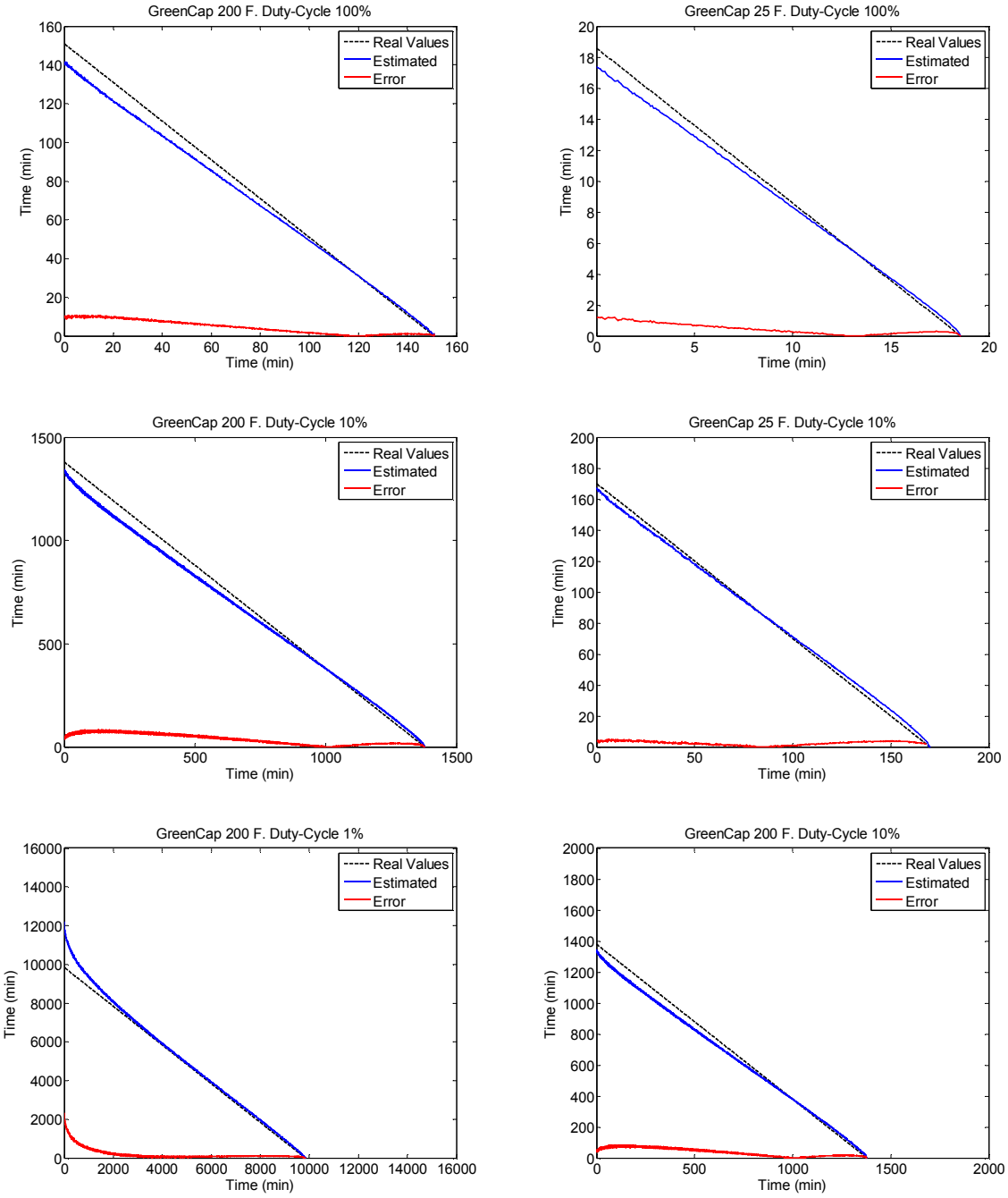

Figure 5.16: *Comparison between the predicted values and the real results for the sensor node's lifetime.*

5.3 Comparison and Discussion

In this final section of the chapter, both the theoretical results obtained with the energy model and the real results obtained with the power supply circuit for the Iris sensor node will be compared and discussed.

Figure 5.5 shows a simulation of the energy levels in the different GreenCaps for the three first days of the year. For a duty-cycle of the sensor node of 1% and 10%, it is demonstrated that even under the worst weather conditions the Iris sensor node can operate without human intervention or servicing. For most wireless sensor network applications where duty cycle is 1% or less, this power supply system is able to provide perpetual operation. The theoretical results showed in Figure 5.5 indicate that it is possible to replenish the energy of a GreenCap of 200 F during the first of January even with cloudy sky, so it is possible to replenish the energy of any GoldCap of GreenCap presented in this work. Moreover, with a duty-cycle of 1% any of the GreenCaps or GoldCaps provides enough energy so that the sensor node could run without incoming energy for at least one day.

For the realistic results of the harvested energy the circuit displayed in Figure 5.15 has been used. The scenario of our test has been seven days with the solar cell connected to a GreenCap of 50 F like it is shown in Figure 5.11. Even if the sky is cloudy the solar cell charges the supercapacitor in a few hours. When the voltage of the supercapacitor increases to 2.4 V the charge stops due to the protection diodes. During all the time that the system have been running, the energy level of the supercapacitor has always been higher than 100 Joules, which assures at least a sensor node's lifetime of 20 hours in case of no incoming energy.

We tested our Discharging Unit using the driver described in Chapter 3, with different duty-cycles (1%, 10% and 100%) and different supercapacitors (GoldCaps and GreenCaps). The theoretical and the real sensor node's lifetime for the different supercapacitors and different duty-cycles are recapitulated in Table 5.4.

Table 5.4: *Sensor node lifetime for different the GoldCaps and GreenCaps*

		GoldCap		***GreenCap***			
		22 F	***50 F***	**25F**	**50F**	**100F**	**200F**
D-C 100%	***Realistic***	*10*	*22*	*15*	*30*	*59*	*120*
	Theoretical	10	21	16	32	64	129
D-C 10%	***Realistic***	*83*	*207*	*170*	*350*	*560*	*1380*
	Theoretical	102	200	159	320	630	1270
D-C 1%	***Realistic***	*600*	*1800*	*1190*	*2540*	*4185*	*9840*
	Theoretical	940	1838	1459	2920	5837	11675

The differences between the real and the theoretical results are due to the next factors: the small variation of the DC-DC converter efficiency in function of the input voltage, the leakage current of supercapacitors, and the possible variation of ±20% between the real values of the supercapacitors and their nominal values.

These differences vary in function of the duty-cycle. For a duty-cycle of 100% the difference between the values are small because of the variation of the voltage converter efficiency and the difference between the nominal values of the supercapacitors and the real value. For a duty-cycle of 1% the error is higher due to the effect of the leakage current is more important in this case.

If we obtain the lifetime of the sensor node for different values of the initial voltage in the supercapacitor, as it is shown in Figure 5.16, this difference becomes smaller when the supercapacitor voltage decreases, so for the cases when the supercapacitor is not fully charge the effect of the leakage current is not important for the prediction of the sensor node lifetime. Thereby, the theoretical models developed are valid to estimate the sensor node lifetime.

Chapter 6

Conclusion

During the last years, renewable energy harvesting has emerged as a viable option to replace battery supplies in energy constrained systems. However, nowadays only a few works developed use energy aware systems. In this work, we analyzed an existing power supply system for an Iris sensor node and developed the energy models necessaries for the prediction of the future estate of energy knowing the actual estate of energy.

Theoretical models have been developed in order to estimate the energy in the supercapacitor depending on the incoming and outgoing energy. These models have been compared with the results obtained with the real circuit and the comparison proves the validity of those models to estimate the energy in the supercapacitor. The incoming energy in function of the environmental conditions has been obtained theoretically. A test circuit has been made to compare the theoretical results with the real ones, and the comparison shows that the theoretical models are valid to estimate the incoming energy

Four GoldCaps and another four GreenCaps have been tested in order to compare their behavior, and also to prove the theoretical models adjust the real results. The theoretical results are in line with the real results, even when the simple model that does not take into account the leakage current of the supercapacitors. Also a software module have been developed in order to the sensor node will be able to estimate both the energy available in the supercapacitor and the sensor node lifetime. This software module has been tested with the existing power supply circuit.

We illustrated how harvesting aware power management improves energy usage compared to battery aware approaches. We presented the design and performance evaluation of an existing power supply board for an Iris sensor node. The results obtained for the predicted lifetime have been compared with the real lifetime of the sensor node, and the error between both is really small.

Despite the many challenges with using a renewable energy source, we have found the experience liberating in many ways: even though the system can only operate at a 1% to 10% duty-cycle, we no longer worry about energy replenishment at a node level. The predictability of daily operation has enabled us to understand what components are the best for maximizing the duty-cycle of the sensor node.

The existing implementation of the power supply circuit uses an energy storage system consisting of a supercapacitor connected to a DC-DC converter to provide a constant and stable output voltage. The sensor node, through the use of a Status Unit, has full knowledge of energy level in the supercapacitor and makes efficient use of available energy resources.

With the use of the software developed, it is possible to know the state of energy of the supercapacitor and predict the sensor node lifetime, and so the applications that run in the sensor node can adjust the duty-cycle in order to avoid that the sensor node dies when the energy level is too low. The models developed works correctly in the scenario where we have test the real circuit. Instead, there are other scenarios where these models need to be adjusted. For example, in places where the variation of the temperature is high the behavior of the circuit will be slightly different, so the current models need to be improved. Moreover, improving the scavenging efficiency we can enhance the sensor node lifetime, so we will try different design options in order to upgrade the existing Charging Unit. This will be our future work.

Appendix 1:

The Solar Radiation Model

The amount of solar energy that a certain photovoltaic cell can provide is dependent on several factors. Since solar energy is a natural resource, it is heavily dependent on the environmental conditions which are generally random in nature. To simplify the model, some parameters or conditions were assumed. Firstly, the temperature dependence of the solar energy is assumed to be negligible. The parameter we would focus on is the relationship between time and the amount of energy provided by the photovoltaic cell.

The model that it will be used requires only a few input parameters: elevation above sea level, latitude, day of the year, cloudiness of the sky and Linke atmospheric turbidity factor [53, 54].

Table A1.1: *Parameters used in the solar model [55]*

Location of the Solar Cell	
φ	Geographical latitude [rad]
z	Elevation above sea level [m]
Date-related parameters	
j	Day number (1-365)
δ	Solar declination
ε	Correction of the variation of the sun-earth distance from its mean value
Solar position	
h_0	Solar altitude (angle between the sun and horizon [rad])
A_0	Solar azimuth (angle between the sun and meridian [rad])
Solar radiation	
I_0	Solar constant (1367 W/m^2)
G_0	Extraterrestrial irradiance/irradiation on a surface perpendicular to the solar beam
B_h	Beam irradiance/irradiation on a horizontal surface

K_c Clear-sky index representing a ratio between overcast global irradiance/irradiation (B_h) and clear-sky irradiance/irradiation (B_{hc})

Parameters of the radiation transmission

p/p_0 Correction of station elevation

T_{LK} Linke turbidity factor

m Relative optical air mass

$\delta_R(m)$ Rayleigh optical thickness

A1.1 Position of the Sun

The position of the Sun with respect to a horizontal surface is given by the two coordinates: solar altitude h_0 (an angle between the Sun path and a horizontal surface), and solar azimuth A_0 (horizontal angle between the Sun and meridian - measured from East), and is calculated as follows [56, 57]:

$$\sin(h_0) = C_{31} \cdot \cos(T) + C_{33} \tag{A1.1}$$

$$\cos(A_0) = \frac{C_{11} \cdot \cos(T) + C_{13}}{\left((C_{22} \cdot \sin(T))^2 + (C_{11} \cdot \cos(T) + C_{13})^2\right)^{1/2}} \tag{A1.2}$$

where:

$$C_{11} = \sin\varphi\cos\delta \tag{A1.3}$$

$$C_{13} = -\cos\varphi\sin\delta \tag{A1.4}$$

$$C_{22} = \cos\delta \tag{A1.5}$$

$$C_{31} = \cos\varphi\cos\delta \tag{A1.6}$$

$$C_{33} = \sin\varphi\sin\delta \tag{A1.7}$$

The Sun declination δ *[rad]* is computed according to [58]:

$$\delta = \arcsin\left(0.3978 \cdot \sin\left(\frac{2\pi}{365.25} j - 1.4 + 0.0355 \cdot \sin\left(\frac{2\pi}{365.25} j - 0.489\right)\right)\right) \tag{A1.8}$$

where j is the day number which varies from 1, for January 1st, to 365, for December 31st.

The hour angle *T [rad]* is calculated from the local solar time t expressed in decimal hours on the 24 hour clock as:

$$T = \frac{2 \cdot \pi}{24(t - 12)} \tag{A1.9}$$

Using the equations (4.1) and (4.2) the solar altitude h_0 and the solar azimuth A_0 have been obtained for the city of Hamburg (latitude 53.82º) for two different days of the year, 1st of January and 30th of June. These results are displayed in Figure A1.1. These results show also the number of hours of sunlight for these two days.

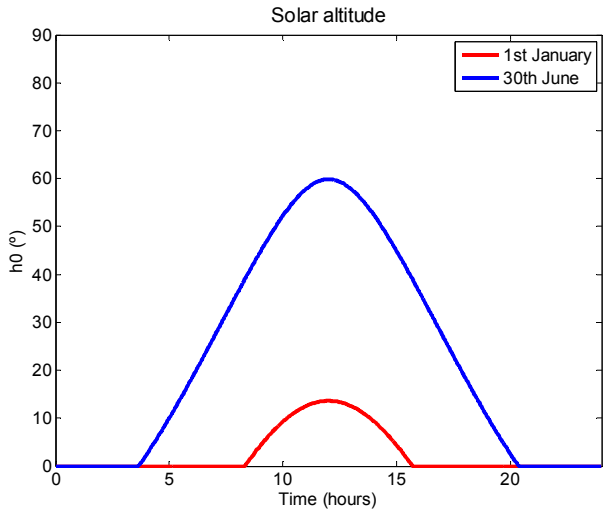

Figure A1.1: *Solar altitude h_0 for January 1st (red line) and for June 30th (blue line)*

A1.2 Clear-Sky Radiation

Outside the atmosphere, at the mean solar distance, the beam irradiance, also known as the solar constant I_0, is 1367 W/m^2. The Earth's orbit is lightly eccentric and the Sun-Earth distance varies slightly across the year. Therefore, a correction factor ε, to allow for the varying solar distance, is applied in calculation of the extraterrestrial irradiance G_0 normal to the solar beam [W/m^2]:

$$G_0 = I_0 \cdot \varepsilon \tag{A1.10}$$

$$\varepsilon = 1 + 0.03344 \cdot \cos(2\pi j / 365.25 - 0.048869) \tag{A1.11}$$

The beam irradiance normal to the solar beam B_{0c} [W/m^2], is attenuated by the cloudless atmosphere, and calculated as follows:

$$B_{0c} = G_0 \cdot \exp\left(-0.8662 \cdot T_{LK} \cdot m \cdot d_R(m)\right) \quad \text{(A1.12)}$$

The term $-0.8662T_{LK}$ is the air mass Linke atmospheric turbidity factor [dimensionless] corrected by Kasten [59]. The Linke turbidity factor characterizes the clearness of the sky. It sums up the effects of the aerosols and water vapor. This factor is approximately 3-3.5 for Europe. The category of services "Climatology" of the SoDa Service provides typical values of T_{LK} for each month, any site. For simulation, one may use the following table [60].

Table A1.2: *Typical values of the Linke Turbidity factor*

	Pure Sky	**Very Clear**	**Clear**	**Summer, with water vapor**	**Polluted (urban or industrial areas)**
TL	1.0	2.0	3.0	5.0	7.0

The parameter m in equation (A1.12) is the relative optical air mass calculated using the formula [58]:

$$m = (p / p_0) / \left(\sin\left(h_0^{ref}\right) + 0.50572 \cdot \left(h_0^{ref} + 6.07995\right)^{-1.6364}\right) \quad \text{(A1.13)}$$

where h_0^{ref} is the corrected solar altitude h_0 (an angle between the sun and horizon) in degrees by the atmospheric refraction component Δh_0^{ref}:

$$\Delta h_0^{ref} = \frac{0.061359 \cdot \left(0.1594 + 1.123 \cdot h_0 + 0.065656 \cdot h_0^2\right)}{1 + 28.9344 \cdot h_0 + 277.3971 \cdot h_0^2} \quad \text{(A1.14)}$$

$$h_0^{ref} = h_0 + \Delta h_0^{ref} \quad \text{(A1.15)}$$

The p/p_0 component in equation (A1.13) is a correction for given elevation z [m]:

$$p / p_0 = \exp\left(-z / 8434.5\right) \quad \text{(A1.16)}$$

The parameter $\delta_R(m)$ in equation (A1.17) is the Rayleigh optical thickness at air mass m and is calculated according to the improved formula by Kasten [59] as follows:

for $m <= 20$:

$$\delta_R(m) = 1/\left(6.6296 + 1.7513 \cdot m - 0.1202 \cdot m^2 + 0.0065 \cdot m^3 - 0.00013 \cdot m^4\right) \quad \text{(A1.17)}$$

for $m > 20$

$$d_R(m) = 1/\left(10.4 + 0.718 \cdot m\right) \quad \text{(A1.18)}$$

The **beam irradiance on a horizontal surface B_{hc} [W/m^2]** is then calculated as:

$$B_{hc} = B_{0c} \cdot \sin(h_0) \quad \text{(A1.19)}$$

where h_0 is the solar altitude angle given by equation (A1.1).

Using the model described in this section the bean irradiance on a horizontal surface B_{hc} have been obtained for the day 1st of January for three different cities with different latitudes: Hamburg (latitude 53.82º), Rome (latitude 41.54º), and Tel Aviv (latitude 32.08º). These results are displayed in Figure 3.2.

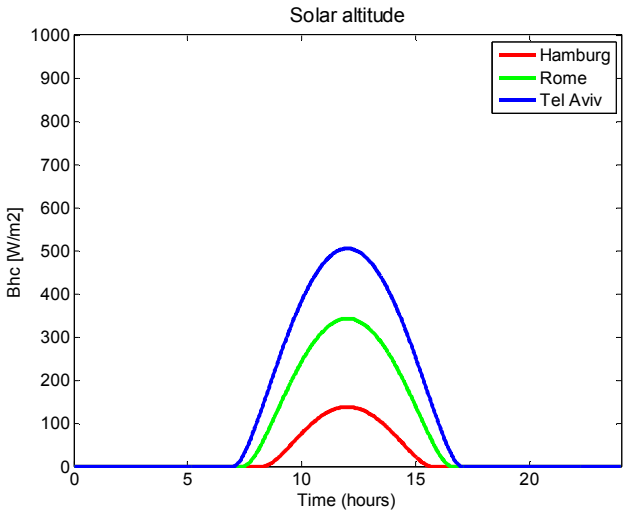

Figure A1.2: *Bean irradiance on a horizontal surface B_{hc} for three different cities: Hamburg, Rome and Tel Aviv.*

A1.3 Radiation Under Overcast Conditions

Overcast radiation can be calculated from the clear-sky values by application of a factor parametrising the attenuation caused by cloudiness. However, the cloudiness observation by a meteorological service routine is usually prone to subjective errors and does not describe sufficiently the physical nature and dynamic spatial-temporal pattern of different types of different types of cloud cover. Therefore a simpler parameter has to be used. For an assessment of global irradiance/irradiation on a horizontal surface for overcast conditions a clear-sky index *Kc* is used [60, 61]:

$$K_c = G_h / B_{hc} \tag{A1.20}$$

The index represents a ratio between global radiation under overcast G_h, and clear-sky G_{hc}, conditions and its values are usually within interval 0.25–1.00. There are several methods of estimation the clear-sky index. Simple regression-based formula for calculation the ratio of global radiation for a given cloud amount G_h, to the clear-sky radiation G_{hc}, can be found. For example, based on the analysis of 10-years hourly records in Hamburg, Kasten and Czeplak [60] have found this empirical equation:

$$K_c = 1 - 0.75(C/8)^{3.4} \tag{A1.21}$$

where C is the cloudiness expressed in okta. The value of C is a random value with the next distribution for latitudes above 40°:

Table A1.3: *Probability function for the Cloud amount [64]*

Cloud Amount (Oaks)	0-2	3-4	5-6	7-8
Probability	0.135	0.068	0.311	0.486

Finally the global radiation under overcast can be expressed as the following equation:

$$G_h = K_c \cdot B_{hc} \tag{A1.22}$$

References

[1] C. Sharp, S. Schaffert, A. Woo, N. Sastry, C. Karlof, S. Sastry, and D. Culler. *"Design and implementation of a sensor network system for vehicle tracking and autonomous interception"*. IEEE EWSN, 2005

[2] A. Arora, P. Dutta, S. Bapat, V. Kulathumani, H. Zhang, V. Naik, V. Mittal, H. Cao, M. Demirbas, M. Gouda, Y. Choi, T. Herman, S. Kulkarni, U. Arumugam, M. Nesterenko, A. Vora, and M. Miyashita. *"A line in the sand: A wireless sensor network for target detection, classification, and tracking.Computer Networks"*, 46(5):605–634, December 2004.

[3] P. Chen, S. Oh, M. Manzo, B. Sinopoli, C. Sharp, K. Whitehouse, G. Tolle, J. Jeong, P. Dutta, J. Hui, S. Shaffert, S. Kim, J. Taneja, B. Zhu, T. Roosta, M. Howard, D. Culler, , and S. Sastry. *"Experiments in instrumenting wireless sensor networks for real-time surveillance"*. International Conference on Robotics and Automation (video), 2006.

[4] P. Dutta, M. Grimmer, A. Arora, S. Bibyk, and D. Culler. *"Design of a wireless sensor network platform for detecting rare, random and ephemeral events"*. IEEE IPSN, 2005.

[5] . Akyildiz, I. F., Su, W., Sankarasubramaniam, Y., Cayirci, E. (2002): *"Wireless sensor networks: a survey"*. Computer Networks, 38: 393–422.

[6] Sakar, S., Adamu: *"A framework for optimal battery management for wireless nodes. IEEE Journal on Selected Areas in Communications"* , 21 (2): 179–188, February 2003.

[7] Boukerche, A. ; Chatzigiannakis, I. ; Nikoletseas, S.: *"Power-Efficient Data Propagation Protocols for Wireless Sensor Networks. In: Simulation Magazine"* (2005)

[8] Pottie, G., Kaiser, W. (2005): *"Principles of Embedded Networked Systems Design"*. Cambridge, UK: Cambridge University Press.

[9] Callaway, E. H. (2003): *"Wireless sensor networks – architectures and protocols"*. Auerbach, Boca Raton, Florida.

[10] Boulis, A., Ganeriwal, S., Srivastava, M. B.: *"Aggregation in sensor networks: An energy-accuracy trade-off"*. In: Proc. 1st IEEE Int. Workshop on Sensor Network Protocols and Applications (SNPA'03), May 2003.

[11] Lin, E.-Y. A., Rabaey, J. M., Wolisz, A: *"Power-efficient rendezvous schemes for dense wireless sensor networks"*. In: Proc. IEEE Int. Conf. on Communications (ICC'04), Paris, France. June 2004.

[12] John A. Stankovic. *"Research Challenges for Wireless Sensor Networks"*. Department of Computer Science. University of Virginia. 2004

[13] Sohrabi, K., Gao, J., Ailawadhi, V., Pottie, G. J. (2000): *"Protocols for selforganization of a wireless sensor network"*. IEEE Personal Communications: 16–27, October 2000.

[14] T. Abdelzaher, B. Blum, D. Evans, J. George, S. George, L. Gu, T. He, C. Huang, P. Nagaraddi, S. Son, P. Sorokin, J. Stankovic, and A. Wood, EnviroTrack: *"Towards an Environmental Computing Paradigm for Distributed Sensor Networks"*, IEEE ICDCS, April 2004.

[15] K. Lahiri, A. Raghunathan, and S. Dey, *"Battery-driven system design: a new frontier in low power design"*, in Proc. IEEE International Conference on VLSI Design, pp. 261–267, 2002.

[16] Z. A. Eu, H. P. Tan, and W. K. G. Seah, *"Routing and relay node placement in wireless sensor networks powered by ambient energy harvesting"* in Proc. of the IEEE Wireless Communications & Networking Conference (WCNC), Budapest, Hungary, Apr 5-8 2009.

[17] S. Roundy, D. Steingart, L. Frechette, P. K. Wright, and J. M. Rabaey, *"Power sources for wireless sensor networks"* in Proceedings of EWSN 2004, Berlin, GERMANY, Jan. 2004.

[18] Crossbow Technology: IRIS Wireless Measurement System. http://www.xbow.com/Products/Product_pdf_files/Wireless_pdf/IRIS_Datasheet.pdf , 2007.

[19] Atmel Products: ATmega1281: Microcontroller with 128K Bytes In-System Programmable Flash. http://www.atmel.com/dyn/resources/prod_documents/2549S.pdf

[20] Crossbow Technology. Mica2 datasheet. www.xbow.com

[21] J.M. Rabaey, M.J. Ammer, J.L. da Silva, Jr., D. Patel, and S. Roundy. *"PicoRadio supports ad hoc ultra-low power wireless networking"*. Computer, 33:42–48, July 2000.

[22] S. Roundy, B. P. Otis, Y.-H. Chee, J. M. Rabaey, and P. Wright. *"A 1.9ghz rf transmit beacon using environmentally scavenged energy"*. IEEE Int. Symposium on Low Power Elec. and Devices, 2003.

[23] T. Voigt, H. Ritter, and J. Schiller, *"Utilizing solar power in wireless sensor networks"*, Proc. IEEE Conference on Local Computer Networks, 2003.

[24] L. Mateu, C. Codrea, N. Lucas, M. Pollak, and P. Spies, *"Energy harvesting for wireless communication systems using thermogenerators"* in Proc. of the XXI Conference on Design of Circuits and Integrated Systems (DCIS), Barcelona, Spain, November 22–24 2006.

[25] Buric, M.P. ; Kusic, G. ; Clark, W. ; Johnson, T.: *"Piezo-Electric Energy Harvesting for Wireless Sensor Networks"*. In: Proceedings of IEEE Annual Wireless and Microwave Technology Conference (WAMICON '06). Clearwater, FL, USA, 2006

[26] S. Roundy, *"Energy Scavenging for Wireless Sensor Nodes with a Focus on Vibration to Electricity Conversion"*. Ph. D. Dissertation, Dept. of EECS, UC Berkeley, May 2003.

[27] A. Kansal, J. Hsu, S. Zahedi, and M. B. Srivastava, *"Power Management in Energy Harvesting Sensor Networks"*, ACM Trans on Embedded Computing Systems, vol. 6, no. 4, September 2007.

[28] Vijay Raghunathan , Aman Kansal , Jason Hsu , Jonathan Friedman , Mani Srivastava, *"Design considerations for solar energy harvesting wireless embedded systems"*, Proceedings of the 4th international symposium on Information processing in sensor networks, Los Angeles, California, 2005

[29] H. Y. Yu, Y. Q. Li, Y. H. Shang, and B. Su, *"Design of a micro photovoltaic system for wireless sensor network"*, J. Functional Materials Devices, vol. 14, no. 1, 2008, to be published.

[30] J. Jeong, X. Jiang, and D. Culler, *"Design and analysis of micro-solar power systems for wireless sensor networks"*, in Proc. of the 5th Intl Conference on Networked Sensing Systems (INSS), Kanazawa, Japan, June 17-19 2008, pp. 181–188.

[31] X. Jiang, J. Polastre, and D. Culler. *"Perpetual environmentally powered sensor networks"*. In Proc. 4th Int. Conf. on Information Processing in Sensor Networks, pages 463–468, Apr. 2005.

[32] K. Lin et al., *"Heliomote: Enabling Long-Lived Sensor Networks Through Solar Energy Harvesting"*, in Proc. of the ACM SenSys, San Diego, CA, USA, November 2-4 2005..

[33] F. Simjee and P. H. Chou, *"Everlast: long-life, supercapacitor-operated wireless sensor node"*, in ISLPED '06: Proceedings of the 2006 international symposium on Low power electronics and design, (New York, NY, USA), pp. 197–202, ACM Press, 2006.

[34] Christopher M. Vigorito, Deepak Ganesan, and Andrew G. Barto *"Adaptive Control of Duty Cycling in Energy-Harvesting Wireless Sensor Networks"*. Department of Computer Science, University of Massachusetts Amherst. 2007

[35] Panasonic, "Panasonic solar cells technical handbook '98/99," http://downloads.solarbotics.com/PDF/sunceramcat.pdf, Aug. 1998.

[36] C. Moser, L. Thiele, D. Brunelli, and L. Benini, *"Adaptive power management in energy harvesting systems"*, in DATE '07: Proceedings of the conference on Design, automation and test in Europe, (New York, NY, USA), pp. 773–778, ACM Press, 2007.

[37] K. Kalpakis, K. Dasgupta, and P. Namjoshi, *"Maximum lifetime data gathering and aggregation in wireless sensor networks"*, Proc. IEEE International Conference on Networking, pp. 685–696, 2002.

[38] L. Gao, R.A. Dougal, and S. Liu. *"Active power sharing in hybrid battery/capacitor power sources"*. In Eighteenth Annual IEEE Applied Power Electronics Conference and Exposition, 2003.

[39] V. Raghunathan et al., *"Design considerations for solar energy harvesting wireless embedded systems"*, in Proc. 4th Int. Symp. Inf. Sensor Netw., 2005, pp. 457–462.

[40] Meteonorm. http://www.meteotest.ch/pdf/am/mn_description.pdf.

[41] Eduardo Lorenzo. *"Solar Electricity Engineering of Photovoltaic Systems"*. Progensa, (1994)

[42] A. Kansal and M. B. Srivastava, *"An Environmental Energy Harvesting Framework for Sensor Networks"*, in Proc. of the Intl Symposium on Low Power Electronics and Design (ISLPED), Seoul, Korea, August 25-27 2003, pp. 481–486.

[43] Panasonic: Gold Capacitors Technical Guid. http://www.panasonic.com/ industrial/components/pdf/goldcap_tech-guide_052505.pdf , 2005.

[44] Samhwa Green-Cap (Electric Double Layer Capacitors). http://www.samwha.com/electric/templatedirs/guest/list_pdf1/DP.pdf

[45] Zhvanetski, O. *"Autonome Solarenergieversorgung mit Superkondensatoren für Drahtlose Sensorknoten"* (Studienarbeit) / Institute of Telematics, Hamburg University of Technology. April 2009.

[46] Ulaby, Fawwaz T. (1999). "*Fundamentals of Applied Electromagnetics"* Upper Saddle River, New Jersey: Prentice-Hall. (1999 ed).

[47] Texas Instruments. Tiny Low Input Voltage Boost Converter: TPS61221. http://www.ti.com/lit/gpn/tps61221

[48] Christian Renner and Jürgen Jessen and Volker Turau, "Lifetime Prediction for Supercapacitor-powered Wireless Sensor Nodes", Proceedings of the 8th GI/ITG KuVS Fachgespräch, Drahtlose Sensornetze (FGSN'09), Hamburg, Germany, 2009

[49] Conrad Solarzelle 5 V/81 mA. http://www.conrad.de/

[50] Lange, C.: *"Energiegewinnung für drahtlose Sensorknoten"* (Diplomarbeit) / Institute of Telecommunications, Hamburg University of Technology. 2008.

[51] Davide Brunelli, Luca Benini, Clemens Moser, Lothar Thiele. *"An efficient solar energy harvester for wireless sensor nodes"*. Proceedings of the conference on Design, automation and test in Europe. Munich, Germany. Pages 104-109, 2008

[52] T. Liu, C. Sadler, P. Zhang, and M. Martonosi. *"Implementing software on resource-constrained mobile sensors: Experiences with Impala and ZebraNet"*. ACM MobiSYS, 2004

[53] Dubayah, R., Rich, P.M., 1995, *"Topographic solar radiation models for GIS"*. International Journal of Geographical Information Systems, 9: 405-419.

[54] Hetrick, W.A., Rich, P.M., Barnes, F.J., Weiss, S.B., *"GIS-based solar radiation flux models"*. American Society for Photogrammetry and Remote Sensing Technical papers. GIS, Photogrammetry and Modeling, 3: 132-143. 1993

[55] Muneer, T., *"Solar Radiation and Daylight Models for Energy Efficient Design of Buildings"*, Oxford (Architectural Press). 1997,.

[56] Krcho, J., *"Morfometrická analýza a digitálne modely georeliéfu"*. Bratislava (VEDA) 1990.

[57] Jenčo, M., *"Distribucia priameho slnečného iarenia na reoreliéfe a jej modelovanie pomocou komplexného digitálneho modelu relief"*. Geografickčasopis, 44: 342-355. 1992

[58] Hammer, A., Heinemann, D., Westerhellweg, A. et al., *"Derivation of daylight and solar irradiance data from satellite observations"*. Proceedings of the 9th Conference on satellite meteorology and oceanography, Paris, May 1998: 747-750, http://www.satel-light.com/core.htm.

[59] Kasten, F., *"The Linke turbidity factor based on improved values of the integral Rayleigh optical thickness"*, Solar Energy, 56: 239-244. 1996

[60] Kasten, F., Czeplak, G., "Solar and terrestrial radiation dependent on the amount and type of cloud. Solar Energy", 24: 177-189. 1980